UCRL-JC-131769
PREPRINT

Crystal Chemical Control of Clinopyroxene-Melt Partitioning in the Di-Ab-An System: Implications for Elemental Fractionations in the Depleted Mantle

C.C. Lundstrom
H.F. Shaw
F.J. Ryerson
Q. Williams
J. Gill

This paper was prepared for submittal to
Geochimica et Cosmochimica Acta

May 5, 1998

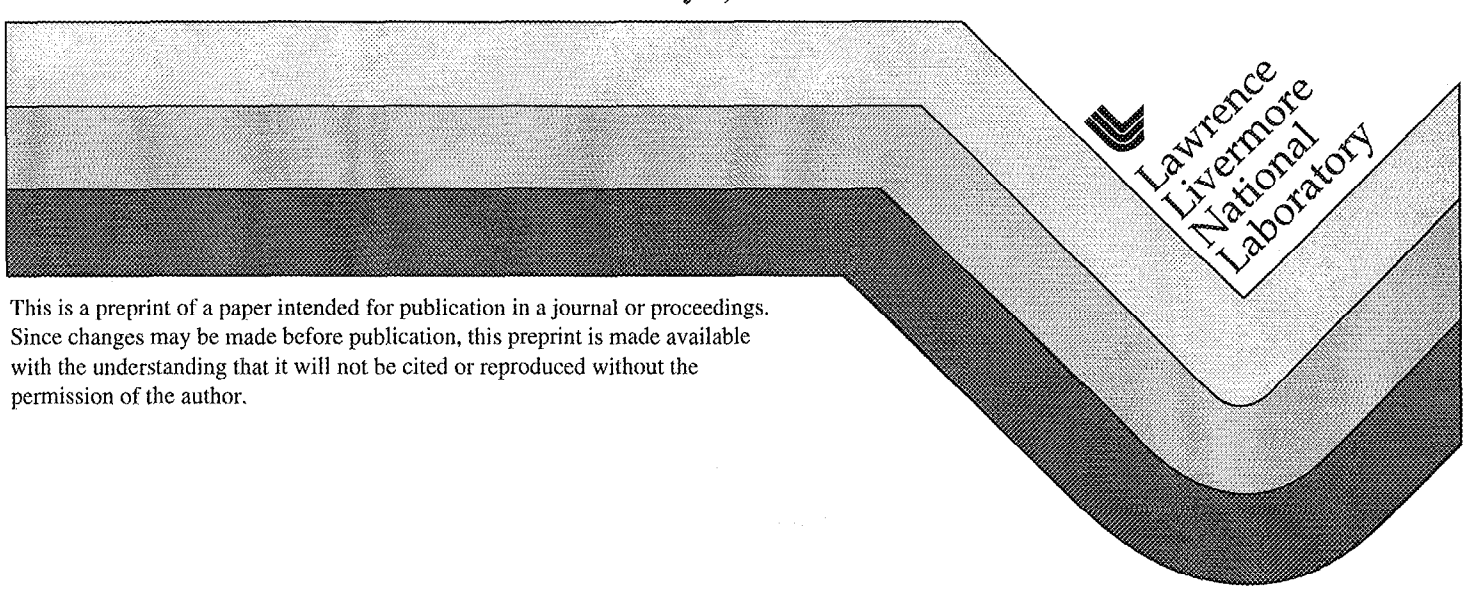

Crystal Chemical Control of Clinopyroxene-Melt Partitioning in the Di-Ab-An System: Implications for Elemental Fractionations in the Depleted Mantle

C.C. Lundstrom[1*], H.F. Shaw[2], F.J. Ryerson[2,3],

Q. Williams[1] and J. Gill[1]

1. Earth Sciences Board, University of California, Santa Cruz, CA 95064
2. Earth Sciences Division, Lawrence Livermore National Laboratory, Livermore, CA 94550
3. Institute of Geophysics and Planetary Physics, Lawrence Livermore National Laboratory, Livermore, CA 94550

*Now at Dept. of Geological Sciences, Brown University, Providence, RI 02912

In Press, *Geochim. Cosmochim. Acta*

Abstract

The partitioning of fifteen trace elements (Rb, Sr, Zr, Nb, Ba, La, Ce, Nd, Sm, Gd, Yb, Hf, Ta, Pb and Th) between clinopyroxene and synthetic melt has been studied in two compositions along an isotherm in the diopside-albite-anorthite ternary at 1 bar pressure. The two compositions correspond to ~$Di_{65}An_{35}$ and ~$Di_{55}Ab_{45}$ and produce clinopyroxenes distinct in chemistry while melt compositions range from 49 wt % SiO_2 to 61 wt. % SiO_2. The partition coefficients of high field strength elements (HFSE) increase by factors of 2 to 8 in Di-An experiments relative to Di-Ab experiments while other elements show very little change (+/- 20%) between compositions. The change in HFSE partitioning correlates with increases in tetrahedral Al_2O_3 (^{IV}Al) content of clinopyroxenes in the anorthite-bearing experiments. Changes in D_{Ta}/D_{Nb} also correlate with ^{IV}Al based on a survey of previously published determinations.

Tests of models of trace element substitution energetics produce values for Young's modulus (E) and optimum D (D_o) consistent with previous results for clinopyroxene for mono-, di- and tri-valent cations. The wide variations in partitioning behavior for tetra- and penta-valent cations are also consistent with these models because the high values for E make partition coefficients and relative HFSE partitioning sensitive to small changes in composition. The overall increase in HFSE partitioning and D_o for the DiAn composition is consistent with D_o increasing as a function of ^{IV}Al, consistent with the role of ^{IV}Al in charge balancing HFSE. However, ^{IV}Al must also cause lattice changes that affect the ability of the clinopyroxene to discriminate between Nb and Ta.

There are two important implications to the observed dependence of HFSE partition coefficients on clinopyroxene aluminum content. First, HFSE will be fractionated from their adjacent REE within ultramafic samples during melting of spinel lherzolite as clinopyroxene Al_2O_3 content decreases. Second, fractionations between Nb and Ta and Zr and Hf observed in mantle derived magmas are consistent with extraction of melt in equilibrium with spinel lherzolite having clinopyroxenes with ~5 wt. % Al_2O_3. The fractionations among HFSE (Nb/Ta, Hf/Zr) and between HFSE and REE observed in both arc magmas and upper mantle peridotites may simply reflect prior depletion by major melting events (F > 10%) which left clinopyroxene as a residual phase. We speculate that the peridotitic sources for MORB and arc lavas are similar in composition with both having significant HFSE anomalies. However, MORB do not typically record HFSE anomalies because of the complementary contribution of HFSE from enriched mafic veins interspersed within the peridotite.

1. Introduction

Understanding the fractionation of trace elements in magmatic systems requires comprehensive knowledge of the partitioning of elements between mineral and melt. Clinopyroxene plays an important role in controlling the fractionation of many trace elements during mantle melting. However, comparison of the results of clinopyroxene-melt partitioning experiments reveal wide variations in the absolute values of trace-element partition coefficients which are often attributed to bulk compositional effects. Recent studies have demonstrated that changes in crystal composition produce large variations in partitioning behavior [McKay et al. 1986; Gallahan and Nielsen, 1992; Lundstrom et al., 1994; Gaetani and Grove, 1995]. Yet, the underlying reasons for the compositional control remain unclear. The relative importance of variations in lattice strain energy caused by size differences between impurity cations and some "ideal" site radius [Onuma, 1968; Blundy and Wood, 1994; Beattie, 1994; Blundy et al., 1996], more complex coupled charge balancing substitutions or a combination of these remains unresolved.

Deciphering the trace element signatures within mantle-derived magmas and ultra-mafic materials requires a complete characterization of mineral-melt partitioning, especially with regard to the relative partitioning of different element groups. Of particular interest to mantle geochemistry is the relative partitioning between high field strength elements (HFSE) and rare earth elements (REE). However, experimental determinations of the partitioning of a large suite of elements between single melt-crystal combinations are few in number [c.f., Hart and Dunn, 1993]. Studies examining multiple compositions (and thereby probing compositional effects on inter-element group partitioning) are even less common [c.f., Skulski et al., 1994]. Therefore, we have investigated the partitioning of fifteen trace elements between clinopyroxene and melt in two binary compositions along an isotherm in the Di-Ab-An system. These experiments are designed to minimize thermal effects on partitioning, and focus strictly on the role of Na and Al contents on clinopyroxene-melt partitioning.

2. Experimental Methods

The experimental techniques used were similar to those of Lundstrom et al. [1994]. Compositions corresponding to ~Di_{65}-An_{35} and ~Di_{55}-Ab_{45} (compared to ~Di_{60}-An_{20}-Ab_{20} in Lundstrom et al., 1994) were prepared from oxides and carbonates with 1 wt.% TiO_2 and 0.2 wt.% Cr_2O_3 added to provide geological realism to the clinopyroxenes as well as to provide direct comparison with previous results of Watson et al. [1987] (Table 1). These materials were ground under ethanol and fused for 4 hours at 1450°C once. Nitrates of trace elements (Th, Rb, Pb, Nb, Ta, Ba, La, Hf, Nd, Sm, Gd and Yb at ~75-650 ppm level) were added to the starting material along with B_2O_3, LiO_2 and $Be(NO_3)_2$ at the <150 ppm level and ground under ethanol. The material was fused and ground an additional two times. Sr and Zr were not added but were present at the 60-100 ppm level due to impurities in the reagents. Li, Be and B results are reported elsewhere [Brenan et al., in press]. The resulting powders were dried, placed into platinum capsules which were welded shut, and run simultaneously in a vertical Deltec furnace. Temperatures were monitored using $Pt/Pt_{10\%}Rh$ thermocouples calibrated against the melting point of Au and positioned at the same vertical level as the sample and to within 5 mm (horizontally) of each sample. Experiments were run by holding the charge in the hot spot of the furnace at 12 degrees above the predetermined liquidus temperature (1281°C) for 24-40 hours, dropping the temperature to the liquidus for 24 hours and ramping at 0.2°C/hr to a final temperature of 1275°C. After three hours at this temperature, the experiments were quenched by dropping them into water. Here, we report the partition coefficients from both starting compositions determined at identical pressure and temperature.

The run products were analyzed for major and trace elements at Lawrence Livermore National Laboratory (LLNL) according to the methods in Lundstrom et al. [1994]. For consistency with Brenan et al. (in press), reported major element compositions reflect the average 10 spots within the clinopyroxenes of each composition and 8 to 10 analyses within each glass (Table 1). In addition, several multi-point traverses were executed to assess clinopyroxene zoning. The partition coefficients reported in Table 2 were calculated by dividing the average ^{30}Si-normalized count rate of each measured isotope in the clinopyroxene (9-12 spots in each experiment) by the average ^{30}Si-

normalized count rates in the glass (6 spots in each experiment) and correcting for the difference in Si content of the two phases assuming equal ion yields for glass and crystals. Errors in Table 2 reflect the combination of the standard deviations on numerous spots of analysis for both the glass and the clinopyroxene. Depending on the element, the standard deviation of repeat analyses of the clinopyroxene exceeded the counting statistics error on the individual analyses by up to a factor of 10 indicating the control of compositional variations within the clinopyroxene. Because Al, Na, and trace element data were collected simultaneously using the ion probe, the role of variations in Al and Na within clinopyroxene could be assessed at each analysis site. Although the compositional variation that we discuss can be observed between the two starting compositions, we also present data as individual spots to better illustrate the close coupling between non-quadrilateral pyroxene components and trace element partitioning. Reported trace element concentrations were determined by calibration against the ^{30}Si normalized count rates on a suite of silicate mineral and glass standards. We estimate an error of ±20% on the concentrations.

3. Results

The experimental runs produced bright green, euhedral, inclusion-free chromian diopsides up to 300 μm in length coexisting with homogenous pale green glasses (Figure 1). From visual observation, the extent of crystallization was low (5-10%); this is confirmed by mass balance ("F" in Table 1) and the similarity between glass and starting compositions. Thus, crystallization-induced shifts in the composition of the melt were negligible. Zoning of clinopyroxenes resembles that in the clinopyroxenes of Lundstrom et al. [1994] having cores richer in Cr_2O_3 (Fig. 1b), but the changes here are less severe than in the previous study. This is likely due to the lower cooling rate used in these experiments during the crystal growth step.

The major element compositions of the average clinopyroxenes and glasses are given in Table 1. The glass in the Di-An composition contained ~49 wt. % SiO_2 while that in the Di-Ab composition contained ~61 wt. % SiO_2. The Na_2O concentration varied from 5 wt. % in the Di-Ab glass to only trace levels in the Di-An glass. Correspondingly, the non-bridging oxygen to tetrahedral

cation ratio (NBO/T) decreased from 0.93 in the Di-An composition to 0.71 in the more polymerized DiAb composition.

The two compositions produced chemically different clinopyroxenes, particularly in the non-quadrilateral components. In the Di-Ab composition, the aluminum contents of the clinopyroxenes were less than 1 wt % with most of the Al_2O_3 residing in the M1 site. The Cr_2O_3 content ranged from 1.5-2.0 wt % and the TiO_2 content averaged 0.22 wt %. Based on site occupancies in the Di-Ab composition clinopyroxenes, Na and Cr co-vary, implying these elements substitute as a ureyite component. In contrast, the clinopyroxenes of the Di-An experiment had ~5 wt. % Al_2O_3. Variations in the Al_2O_3 content of the clinopyroxene reflect variations of Al in the tetrahedral site (^{IV}Al) with no observed change in octahedral Al (Fig. 2). Like the clinopyroxenes of the experiments of Lundstrom et al. [1994], Cr_2O_3 (1.9-2.8 wt %), TiO_2 (0.32-0.5 wt %) and Al_2O_3 co-vary with clinopyroxene cores richer in Cr, Ti and ^{IV}Al (Fig. 2). Thus, we observe a fundamental difference in the TiO_2 and Al_2O_3 contents of clinopyroxenes produced from bulk compositions that vary primarily in only their alkali content with no difference in temperature.

Clinopyroxene-melt partition coefficients calculated for the average clinopyroxene compositions are presented in Table 2 along with glass trace element concentrations. The ratio of the partition coefficients of the Di-An composition to those in the Di-Ab composition is also given. While REE and alkalis have essentially the same partition coefficients in the two compositions, the partitioning of HFSE changes dramatically between the two endmembers (Table 2, Fig. 3).

Although we have not varied the concentration level of trace elements in these experiments to verify that Henry's law behavior is obeyed, concentration levels are similar to those in our previous experiments in the Di-Ab-An system [Lundstrom et al., 1994] which demonstrated Henry's Law behavior for a variety of trace elements at a similar temperature. Approach to equilibrium in these experiments is indicated by the relative homogeneity of crystals and glass, and by partition coefficient-clinopyroxene composition correlations similar to those of Lundstrom et al. [1994], in which equilibrium was demonstrated through reversal experiments. In addition, our measured partition coefficients for highly incompatible elements, Ba and Rb, are as low or lower than any thus

far published for clinopyroxene-melt equilibrium. Failure to attain/approach equilibrium will bias partition coefficients towards unity; the low and consistent values for the partitioning of these highly incompatible elements suggests that equilibrium was likely to have been attained at the crystal-liquid interface at all times.

3.1 Comparison to Previous Studies

Mineral-melt partition coefficients vary as a function of mineral and melt composition and intensive variables. The large range reported for the partitioning of HFSEs between clinopyroxene and melt is the result of such variations (Table 3). Our results, in which the effect of intensive variables has been eliminated, manifest a similarly large range in $^{cpx/melt}D$, highlighting the effects of compositional variations. Results for individual spot partition coefficients, combined with previous results [Lundstrom et al. 1994], suggest that much of the observed variation relates to crystal chemical controls produced by non-quadrilateral component substitutions in pyroxene. Each of the high field strength elements have substantially higher partition coefficients in the DiAn experiments with the partition coefficients of individual spots increasing as a function of the Al_2O_3 content of clinopyroxene (Fig. 4a). Because the Al_2O_3 variation relates solely to ^{IV}Al (Fig. 2), the observed increase in $^{cpx/melt}D_{HFSE}$ in the DiAn composition results from increases in ^{IV}Al.

Our results imply that partitioning between clinopyroxene and melt can fractionate Nb from Ta and Zr from Hf. D_{Nb} is correlated with D_{Ta} for individual spots indicating that these two elements have similar substitution behavior; however, the slope greater than 1 indicates that Ta can be fractionated from Nb with increasing aluminum content of the clinopyroxene (Fig. 5). Indeed, all studies with combined D_{Nb} and D_{Ta} data show that D_{Ta}/D_{Nb} increases with ^{IV}Al (Fig. 5). Additionally, we have found significant differences in the partitioning of Hf and Zr between clinopyroxene and melt with a D_{Hf}/D_{Zr} of near 2. Results of Skulski et al. [1994], Johnson et al. [1989], Fujinawa and Green [1997] and Hart and Dunn [1993] are in accord with this result.

In general, our results for REE partitioning between clinopyroxene and melt compare favorably with the numerous other studies and produce a pattern that is similar to previous

clinopyroxene-melt results. The pattern is flat between Sm and Yb with D_{Sm} being identical within error to D_{Yb} and D_{Gd}. Recent results for REE partitioning suggest a dependence of D_{REE} on the CaTs component of the clinopyroxene with D_{Ce} increasing by a factor of two and D_{Yb} increasing by a factor of 2.5 as X_{CaTs} varies from 0.03 up to 0.23 [Gaetani and Grove, 1995]. Our values of X_{CaTs} range from 0.00 to 0.07, and our D_{REE} only show at most a 20% increase across this range.

Our values for D_{Pb}, D_{Th}, D_{Sr}, and D_{Ba} also agree well with previous results. Ray et al. [1983] studied the partitioning of Sr and Ti along several isotherms in the Di-Ab-An system, with the only difference from our experiments being our inclusion of Cr_2O_3 and TiO_2 (at the 1 wt % level). Notably, they also observed a similar increase in D_{Sr} and a small but noticeable decrease in D_{Ti} with increase in Ab component of the system, consistent with the results here. However, their clinopyroxenes had a much smaller range in Al_2O_3 content (0.54-1.46) probably due to the lack of Cr_2O_3 in the starting composition. Our results for Sr, Ba and Pb partitioning are in good agreement with our previous results (0.1, 0.0002 and 0.009 respectively) [Lundstrom et al., 1994] and those of Beattie [1993] (average values of 0.086, 0.00029, and 0.007, respectively). Few results have been reported for D_{Rb}. Our results (0.00021-0.00024) are considerably lower than those of Shimizu [1974] (0.001-0.004) and Hart and Brooks (phenocryst/matrix = 0.0018) [1974].

4. Discussion

4.1. Compositional Controls on Clinopyroxene-Melt Partitioning

Our data can be used to compare the relative effects of liquid structure variations versus crystal chemical changes on trace element partitioning because temperature and pressure are constant. Liquid-liquid partitioning experiments [c.f., Ryerson and Hess, 1978] imply that the increased polymerization of the Di-Ab melt, evidenced by lower NBO/T, should result in less incorporation of TiO_2 into the melt. Therefore, if liquid structure is the dominant control on clinopyroxene-melt partitioning, D_{Ti} should be higher in the Di-Ab composition; however, the opposite is observed indicating the predominant role of crystal chemical control.

Between the DiAb and DiAn melts, the major compositional variant is the substitution of $NaAlO_2$ for $Ca_{0.5}AlO_2$, and it can be argued that the lower Al_2O_3 content of clinopyroxenes in the DiAb composition reflects the decreased activity of Al_2O_3 in the DiAb melt resulting from this substitution. The observed compositional dependence of HFSE partitioning could therefore reflect the increased activity of Al_2O_3 in the DiAn melt. However, several lines of evidence refute this. First, the correlation between the HFSE partition coefficients and ^{IV}Al of the clinopyroxene (Fig. 2,4,5) is observed not only between the DiAb and DiAn compositions, but also solely within the DiAn data which are sodium-free, and unaffected by changing speciation of aluminum in the melt. The low degree of crystallization argues that melt Al_2O_3 did not change significantly during crystal growth in our experiments; however, if it did, Al_2O_3 at the crystal melt interface would increase, not decrease (arguments detailed in Lundstrom et al. [1994]). Therefore, changes in Al_2O_3 activity in the melt are not likely to account for our observations within the DiAn composition. Other experimental data also implicate crystal chemical control. REE partition coefficients closely track clinopyroxene Al_2O_3 content within a sodium free system where melt Al_2O_3 is essentially constant [Gaetani and Grove, 1995]. HFSE contents correlate with Al_2O_3 within clinopyroxenes formed in hydrous fluid-clinopyroxene partitioning experiments where fluid content should not have changed [Brenan et al., 1995]. Lastly, in contrast to the observed discrimination of HFSE during clinopyroxene-melt partitioning (D_{Ta}/D_{Nb} and D_{Hf}/D_{Zr}), the similarity of solution behavior of Zr and Hf in high silica melts also suggests that liquid state variations are unlikely to cause fractionation of such element pairs [Ellison and Hess, 1986].

Mineral-melt partitioning, and in particular inter-element fractionation among isovalent groups, has been related to the microstructural strain associated with placing a cation into a crystallographic site where a misfit in size relative to some "ideal" cationic radius occurs [Beattie, 1994; Blundy and Wood, 1994; Wood and Blundy, 1997]. These treatments provide a physical basis for the long observed parabolic correlations between partition coefficient and ionic radius [Onuma et al., 1968]. Given the large variation in the partitioning of certain elements seen between our two compositions, it is useful to examine the degree to which these treatments can explain our

observations. Therefore, we have used the equations of Blundy and Wood [1994] to calculate differences in optimum D (D_o) and Young's modulus (E) for our two compositions.

For mono-, di- and trivalent cations, we assume the same site occupancies (substitution in the M2 site) as Blundy and Wood [1994] and use an optimum radius (r_o) for the M2 site based on equation 15 of Wood and Blundy [1997]. By plotting ln (D) versus $[r_o(r_i-r_o)^2/2 + (r_i-r_o)^3/3)]$ [e.g., LaTourette et al., 1995] (r_i is the ionic radius of the element), we obtain E and D_o by linear regression. We omit Pb because this description does not incorporate effects associated with the electronic structure of this ion [Blundy and Wood, 1994]. Our results for these regressions, plotted with our data in Fig. 6, are similar to the results of Blundy and Wood [1994] (Table 4).

The partitioning of divalent cations into M2 provides a good illustration of the control on partitioning by site size energetics (Fig. 6). The linearized regressions for Ca, Sr and Ba in both compositions produce excellent fits (Table 4), yet produce very different slopes and intercepts indicating a change in E and D_o. In both compositions, Ba is equivalently incompatible but D_{Ca} varies significantly. From these two regressions, it is clear that the increase in partitioning of Sr in the DiAb composition can be explained by the change in D_o which is approximated by the partitioning of Ca. Regressions for both compositions predict ${}^{cpx/melt}D_{Ra} \sim 1 \times 10^5$.

The partition coefficients for Ti, Hf and Zr have been used to obtain E, D_o and r_o for the tetravalent cations. We obtain best fits to the data using r_o of 0.66 Å for the DiAn composition and 0.652 Å for the DiAb composition (Table 4). The inferred values for E of the two compositions are similar and consistent with the large values expected for small, highly charged cation sites, ~30,000 kb for Ti-Hf-Zr in the M1 site *vs.* ~3000 kb for the REEs in the M2 site. D_o changes from being incompatible in the DiAb composition to compatible in the DiAn composition, consistent with the higher D_{HFSE} observed in the DiAn composition.

The results for Th fall well off the Ti-Hf-Zr regression indicating that its ionic radius (1.05 Å) is too large for incorporation in the M1 site. However, its radius is very close to the value of r_o for the M2 site. The radius of Th is equivalent to that of Gd which has the largest partition coefficient for the REEs measured in this study. As such, the partition coefficient for Th approximates D_o for

quadravalent cations on the M2 site. Given the smaller ionic radius of U^{+4} [Shannon, 1976], this result predicts the incompatibility of U^{+4} relative to Th observed for clinopyroxene-melt equilibrium [LaTourrette and Burnett, 1992; Beattie, 1993; Lundstrom et al., 1994] for diopsidic clinopyroxenes.

Two partition coefficients for pentavalent cations (Ta and Nb) are not sufficient to independently constrain D_o, E and r_o. However, inferences from other isovalent groups suggests that the partitioning of these cations may be very sensitive to small changes in clinopyroxene composition. For instance, it has been demonstrated that E for mono-, di- and trivalent cations in clinopyroxene and plagioclase varies linearly with valence [c.f., Wood and Blundy, 1997]. Extrapolating the E (M1) for quadravalent cations suggests E ~38,000 kb for pentavalent cations on that site, which will manifest itself as a very tight parabola on plots of partition coefficients versus ionic radius. The ionic radii of Nb and Ta are essentially equal (0.64 Å) although Ta is likely slightly smaller than Nb based on analogy to Zr-Hf. These radii fall quite close to the value of r_o for the M1 site defined by the Ti-Hf-Zr regression (0.65-0.66 Å). As such, we would expect that small variations in r_o with composition could result in strong inter-element fractionation, or even reversals in the sense of fractionation. These indications are supported by our data and Fig. 5 in which D_{Ta}/D_{Nb} varies as a function of clinopyroxene composition.

The data imply that HFSE partitioning between clinopyroxene and melt is sensitive to clinopyroxene Al_2O_3 content in two ways. First, there is an overall increase in D_{HFSE} as ^{IV}Al increases. Second, there is increased fractionation of Nb and Ta with increased ^{IV}Al. These two sensitivities probably reflect the dual role of ^{IV}Al in affecting both the ability to charge balance high valence cation incorporation and the distortion of M1 lattice sites as the chains of silica tetrahedra are altered.

With increasing ionic charge, charge balancing mechanisms in minerals become more important. Highly charged cations require more complicated charge balancing mechanisms than those required for mono-, or trivalent cations, so their substituting behavior is likely to be sensitive to changes in clinopyroxene chemistry that facilitate charge neutrality. ^{IV}Al is the most likely mechanism for charge balancing HFSE since Na in the M2, the other possible mechanism, is not supported by

the data (DiAb cpx with greater Na contents show the least ability to incorporate HFSE). Based on the observed higher value for D_o in the DiAn composition and the clear correlation between D_{HFSE} and ^{IV}Al, the value of D_o, which sets the absolute vertical position of the parabola, is likely to be a function of ^{IV}Al. Further support for this interpretation comes from the observation that Th also strongly depends on ^{IV}Al despite occupying a different lattice site (M2).

However, since Nb and Ta have identical charge balancing requirements, the differences in their D's as a function of ^{IV}Al (Fig. 5) cannot reflect charge compensation but rather implies that lattice parameters also vary with ^{IV}Al. Understanding how variations in ^{IV}Al affect lattice structure and HFSE partitioning is not straightforward. The clinopyroxene M1 site changes in response to ^{IV}Al variation. The CaTs component reduces the average M1-O bond length by 0.13 Å and increases the standard deviation on the M1-O bond length by a factor of two from pure diopside to pure CaTs [Smyth and Bish, 1988]. Thus, both the overall size and the amount of distortion of the octahedral site will change with increased ^{IV}Al. Shifts in site size are reflected in r_o; because of the large values for E, small shifts in r_o can readily change relative partitioning. Although speculative, increased site distortion may also lead to greater selectivity between similarly sized HFSE (i.e. Nb and Ta) especially if highly charged cations favor off-center ion positions.

Thus, site size energetics provide a useful means for explaining the observed relation between partition coefficients and ionic radii [Onuma et al., 1968] and appear to describe one of the major controls on trace element partitioning. We have documented the dependence of clinopyroxene-melt partitioning of HFSE on ^{IV}Al of the clinopyroxene. Since increased ^{IV}Al provides more ability to charge balance HFSE, higher D_{HFSE} and higher D_o result. At the same time, increased ^{IV}Al must affect the site geometry because charge balancing cannot explain the Nb-Ta fractionation observed. Because E is large for quadra- and pentavalent cations, shifts in r_o due to composition or distortions in site geometry can manifest themselves in large changes in relative partition coefficients, accounting for the extreme selectivity of partitioning between elements of nearly identical radii.

4.2. Implications for the depleted mantle and mantle derived magmas

Aside from being iron-free, the clinopyroxene compositions of these experiments strongly resemble chromian diopsides found in mantle peridotite samples while the liquid compositions range from haplobasaltic to haplotonalitic. Our results, particularly the observed partitioning dependence on clinopyroxene aluminum content, are highly relevant to mantle-melt partitioning and the chemical evolution of upper mantle geochemical reservoirs. There are two important but distinct ramifications of the compositional control of Al on HFSE partitioning relevant to mantle geochemical observations.

First, because the Al_2O_3 contents of abyssal peridotite pyroxenes reflect the amount of basaltic melt extracted [Dick et al., 1984; Dick and Fisher, 1984; Michael and Bonatti, 1985; Niu and Hekinian, 1997a], the observed partitioning dependence on pyroxene Al_2O_3 content will be important to incompatible element systematics as peridotite is progressively depleted. As Al_2O_3 decreases, the relative partitioning of the REE, HFSE and large-ion-lithophile (LIL) groups of elements will vary depending on the depth of melting and degree of depletion of the peridotite.

Studies of peridotite xenoliths, alpine massifs, and abyssal peridotites document that the mantle is chemically heterogeneous on a variety of scales and it is difficult to discern long-lived source variations from melting processes. With improved microanalytical techniques, it has become evident that some ultramafic samples have been depleted to extreme extents in incompatible trace elements in general and the HFSE in particular [Johnson et al., 1990; Salters and Shimizu, 1988]. Ti and Zr deficiencies relative to their adjacent REE on normalized incompatible element plots, often denoted as Ti/Ti* and Zr/Zr*, are commonly found in abyssal peridotites as well as in many ultramafic samples from the mantle [Johnson et al., 1990; Salters and Shimizu, 1988]. Thus, the bulk partition coefficients for Ti and Zr during some prior fractionation appear to have differed from those of their adjacent REE.

The inferred shift resembles the changes in partitioning observed in our experiments and may relate to the decrease in Al_2O_3 in clinopyroxene with increased degree of melting. For instance, at moderately high Al_2O_3 contents (5 wt %), our results show that $D_{Sm} > D_{Zr} > D_{Nd}$ which is in accord with the order of these elements on incompatibility diagrams [Sun and McDonough, 1989]. However, as the Al_2O_3 content decreases, the order of partitioning changes to $D_{Sm} > D_{Nd} > D_{Zr}$.

Thus, melting of clinopyroxenes of lower Al_2O_3 content will dramatically change the observed HFSE/REE behavior and can produce the Zr anomalies ($Zr/Zr^* < 1$) observed in mantle peridotites. Clinopyroxenes from refractory abyssal peridotites have Al_2O_3 contents of ~3 wt % which would correspond to D_{Sm}/D_{Zr}~2, resulting in Zr deficits relative to Sm and Nd. Similarly, Ti shifts with composition from being more compatible than middle and heavy REE to being slightly less compatible. Although the partition coefficient shifts in this study cannot account for large Ti deficits, it is clear that Ti is readily decoupled from the adjacent REE with relatively minor shifts in clinopyroxene composition. Lastly, Sr is generally considered similar in incompatibility to Ce during mantle melting. However, both large enrichments and depletions of Sr relative to Ce are found in melt inclusions and some magmas [Sobolev and Shimizu, 1993; Gurenko and Chaussidon, 1997]. Such anomalies are consistent with our observed 30% change in Sr partitioning as a function of clinopyroxene composition. However, in contrast to HFSE partitioning, D_{Sr} increases as clinopyroxene Al_2O_3 content decreases. Notably, Gurenko and Chaussidon [1997] find positive Sr anomalies in the most depleted melt inclusions within olivines in Icelandic tholeiites, consistent with derivation from an ultra-depleted mantle where Sr has been retained relative to REE through a chemically-induced increase in partition coefficient.

A second implication of our measured partition coefficients is the fractionation among HFSEs during melting of spinel lherzolite with moderate aluminum contents. Analytical improvements have facilitated low concentration HFSE measurements documenting that Hf-Zr and Nb-Ta fractionations occur in the mantle [Plank and White, 1995; Niu and Batiza, 1997; Niu and Hekinian, 1997b; Eggins et al., 1997]. Our partitioning data can be used to assess how these deviations could be produced. For instance, both Plank and White [1995] and Niu and Batiza [1997] show that depleted island arc tholeiites, near-ridge seamount basalts and depleted MORB show a dramatic decrease in Nb/Ta with decreasing Nb (Fig. 7a). This behavior is not compatible with variations in degree of melting but rather reflects previous depletion in the source for these basalts [Plank and White, 1995]. The previous depletion is consistent with the fractionation of Nb and Ta predicted by clinopyroxene-melt partitioning at moderate Al_2O_3 contents. Using our DiAn partition coefficients, the most depleted

magma observed can be modeled as a 12% batch melt from a solid previously having lost a large degree (12%) batch melt from an originally "primitive mantle" [Sun and McDonough, 1989]. It is also possible that garnet could be responsible for Nb/Ta fractionation but garnet need not be invoked [Green et al., 1989].

The observed data array extending to higher Nb/Ta (Fig. 7a) probably reflects the addition of small amounts of melt derived from a trace-element enriched source, such as mafic veins interspersed within peridotite [Allegre and Turcotte, 1986; Hirschmann and Stolper, 1996]. We have modeled the Nb/Ta trend as a mix between average OIB (as a proxy for enriched vein melts) [Sun and McDonough, 1989] and the most depleted basalt observed. The observed primitive basalts [Plank and White, 1995; Niu and Batiza, 1997] reflect the addition of small amounts (1-2%) of OIB-like melts (Fig. 7a) while the majority of MORB, being non-primitive with higher concentrations of incompatible elements, require 5-10% contamination by OIB-like melts. Because of the strong contrast in incompatible element concentrations between the two sources, most oceanic basalts (MORB and OIB) reflect the domination of the OIB endmember in fixing the Nb/Ta ratio near chondritic values.

Similarly, our partition coefficients can explain the fractionation of Zr and Hf observed in mantle derived basalts (Fig. 7b). Using the same two stage model (two 12% batch melts of primitive mantle) [Sun and McDonough, 1989] as our Nb/Ta model, the most depleted Zr/Hf ratio observed is reproduced (Fig. 7b). In contrast with Nb/Ta, the higher bulk partition coefficient for Hf results in a significant increase in Zr/Hf_{melt} even at 12% melting. The observation of many super-chondritic Zr/Hf ratios but far fewer (with less deviation) super-chondritic Nb/Ta ratios agrees with the relative magnitudes of the partition coefficients measured in this study. As our models illustrate, a change of Nb/Ta_{melt} relative to Nb/Ta_{source} is unlikely to occur except at very small degrees of melting whereas moderate degrees of melting will produce fractionation of Zr/Hf relative to the source.

Similar to Nb/Ta, we have attempted to model the observed Zr/Hf data as a mix between the most depleted basalt observed and average OIB [Sun and McDonough, 1989]. However, average OIB cannot account for the observed higher values of Zr/Hf nor does it appear to accurately represent

the Zr/Hf of some OIB (Fig. 7b). For example, the average of Zr/Hf of primitive alkalic basalts (<45% SiO_2) from the Canary Islands is 43 with Zr/Hf as high as 52 [Hoernle et al., in prep]. Therefore, we assume an endmember equal to Sun and McDonough [1989] in [Zr] but with a Zr/Hf of 48. In reality, different OIB endmembers may well have different Zr/Hf [Weaver, 1991]. Using this endmember, typical MORB reflects a mix of 10% of this enriched component with a melt derived from a previously depleted mantle. Thus, the Zr-Hf data are also consistent with prior depletion of upper mantle peridotite followed by mixing during magma production.

The mantle normalization diagram provides a useful method for evaluating the extraction of elements from the bulk mantle. Especially in the case of MORB where crustal level mixing is likely to be very efficient, magma compositions should faithfully reflect the concentrations of highly incompatible elements within the integrated source region prior to melting. However, the models given above (previous source depletion followed by mixing) demonstrate that much of the trace element budget of mantle derived melts may not be derived from the peridotites but rather come from enriched heterogeneities. Indeed, the observation of mixing arrays that are clearly tied to isotopic variation [Niu and Batiza, 1997] provides evidence that variations in incompatible element contents in MORB probably reflect source variation to a greater degree than melting process. Therefore, inferences that recent fractional melting is responsible for observed the Ti/Ti* and Zr/Zr*<1 in abyssal peridotites [Johnson et al., 1990] based on the absence of HFSE anomalies in associated MORB are not definitive. The range of Zr and Ti concentrations within abyssal peridotite clinopyroxenes [Johnson et al., 1990] is more consistent with a fractional melting process, yet there remains considerable uncertainty about the original concentrations prior to melting.

With the exception of arc magmas, high field strength anomalies (depletions in HFSE relative to REE) are not common in mantle-derived melts. The origin of these depletions in arc volcanics has been the subject of numerous proposals but no clearly favored explanation exists [Saunders et al., 1980; Green, 1981; Kelemen et al., 1990; Woodhead et al., 1993, Thirwall et al., 1994]. Woodhead et al. [1993] show that arc HFSE depletions are consistent with a source depleted by back-arc basalt extraction since Ti/Zr increases progressively from more enriched back-arc basalts to more depleted

arc magmas at the volcanic front of the arc. Such a scenario is compatible with geodynamic inferences that mantle upwells beneath the back-arc and moves toward the arc to become the arc source.

The processes discussed above, mixing of melts derived from a heterogeneous mantle and prior depletion of arc sources by back-arc melting, share a commonality which yields a self-consistent view of the upper mantle. Based on our conclusion that the MORB source consists of both peridotite and enriched mafic veins, we suggest that average upper mantle peridotite is substantially more depleted in incompatible trace elements than anticipated from MORB containing significant HFSE/REE anomalies [Salters and Shimizu, 1988] and fractionations between HFSE (Nb/Ta and Zr/Hf). The observed relation between arc and back-arc rocks [Woodhead et al., 1993] reflects the role of decompression melting in the back-arc selectively extracting mafic veins from the mixed source leaving solely peridotite, with its characteristic HFSE depletion, to constitute the predominant source for arc magmas.

Our intent is to emphasize that MORB should not be equated with a solely peridotite source and that the *peridotite* source beneath ridges and arcs may, in fact, be quite similarly depleted; yet, the degree of depletion of the MORB peridotite source is often hidden by mixing. As an example, Elliott et al. [1997] distinguish the Mariana Arc source from the MORB source by observing La/Nb to be a factor of 2 greater than any MORB. However, the observed La/Nb in depleted seamount lavas suggests La/Nb differs little between the Mariana Arc source and what we infer to be the depleted source for MORB melting (Fig. 7c); moreover, based on the same melt extraction model as for Nb/Ta, high La/Nb in the previously depleted peridotite should be expected because of the low value for D_{Nb}. The mixing model shows that very little enriched melt (0.3-1%) is needed to significantly lower La/Nb back to "MORB-like" levels and it is likely that the most depleted melts of Niu and Batiza [1997] do not represent the true depleted endmember. Clearly, other components from the slab are needed to account for the chemical systematics of the Mariana Arc (and arcs in general). Yet, deciphering sources and processes during melting of the upper mantle may require a distinction

between "bulk upper mantle" and "upper mantle peridotite" and a corresponding re-evaluation of the composition of average upper mantle peridotite.

5. Conclusions

The partitioning of trace elements between clinopyroxene and melt under isothermal conditions shows that changes in clinopyroxene chemistry produce important shifts in inter-element partitioning. The partition coefficients of HFSE increase by factors of 2 to 8 due to increased ^{IV}Al in clinopyroxenes whereas other elements show very little change (+/- 20%) between compositions. The relative partitioning of HFSE, D_{Ta}/D_{Nb} for example, also are affected by ^{IV}Al variations.

The clinopyroxene-melt partitioning behavior of mono-, di- and tri-valent cations is well explained by site-size energetics [Blundy and Wood, 1994]. Even the wide variations in partitioning behavior for tetra- and penta-valent cations are consistent with this model because the high values for E make partition coefficients and relative HFSE partitioning very sensitive to small changes in composition. The overall increase in HFSE partitioning and D_o for the DiAn composition is consistent with D_o being a function of ^{IV}Al, consistent with the role of ^{IV}Al in charge balancing HFSE. However, ^{IV}Al must also cause lattice changes that affect the ability of the clinopyroxene to discriminate between Nb and Ta.

The compositional control of clinopyroxene aluminum content may be critical in explaining two geochemical observations within the oceanic mantle. First, the decoupling of HFSE and Sr from the REE observed in both peridotites and melt inclusions may be explained by partition coefficient changes due to decreases in clinopyroxene Al_2O_3 content with progressive melting. Second, depletions of Nb relative to Ta and Zr relative to Hf in mantle derived magmas reflect their peridotite source previously depleted by melt extraction in the presence of residual clinopyroxene having moderate Al_2O_3 contents. The trend of increasing Nb/Ta and Zr/Hf with increasing trace element concentrations observed in mantle derived magmas is consistent with mixing between melts derived from previously depleted peridotite and more enriched sources such as mafic veins. Chemically similar peridotites, depleted in HFSE relative to REE and containing low Nb/Ta and Zr/Hf, constitute

the sources for both MORB and island arcs. However, because MORB reflects integration of its source region, small contributions by vein melts erase the signature of this ultra-depleted peridotite source. In contrast, because enriched veins are effectively removed by back-arc melting, arc lavas more accurately record the depleted nature of upper mantle peridotite including HFSE anomalies.

Acknowledgments

We thank Terry Plank for invaluable discussions on peridotite and basalt trace-element systematics. The manuscript benefited from reviews by T. LaTourrette and R. Nielsen. This work is supported by an IGPP grant to QW, and a NSF-RIDGE post-doctoral fellowship to CCL. FJR and HFS acknowledge the support of the Institute of Geophysics and Planetary Physics at LLNL operating under the auspices of DOE contract ENG-7405.

References

Allegre C. J. and Turcotte D. L. (1986) Implications of a two-component marble-cake mantle. *Nature* **323**, 123-127.

Beattie P. D. (1993) The generation of uranium series disequilibria by partial melting of spinel peridotite: constraints from partitioning studies. *Earth Planet. Sci. Lett.* **117**, 379-391.

Beattie P. D. (1994) Systematics and energetics of trace element partitioning between olivine and silicate melts: Implications for the nature of mineral melt partitioning. *Chem. Geol.* **117**, 57-72.

Blundy J. and Wood B. (1994) Prediction of crystal-melt partition coefficients from elastic moduli. *Nature* **372**, 452-454.

Blundy J. D., Wood B. J., and Davies A. (1996) Thermodynamics of rare earth element partitioning between clinopyroxene and melt in the system CaO - MgO - Al_2O_3 - SiO_2. *Geochim. Cosmochim. Acta* **60**, 359-364.

Brenan J. M., Neroda E., Lundstrom C. C., Shaw H. F., Ryerson F. J., and Phinney D. L. Behavior of boron, beryllium and lithium during melting and crystallization: constraints from mineral-melt partitioning experiments. in press *Geochim. Cosmochim. Acta*

Brenan J. M., Shaw H. F., Ryerson, F. J., and Phinney D. L. (1995) Mineral-aqueous fluid partitioning of trace elements at 900°C and 2.0 GPa - constraints on the trace element chemistry of mantle and deep crustal fluids. *Geochim. Cosmochim. Acta*, **59**, 3331-3350.

Dunn T. (1987) Partitioning of Hf, Lu, Ti and Mn between olivine, clinopyroxene and basaltic liquid. *Contrib. Mineral. Petrol.* **96**, 476-484.

Dick H. J. B. and Fisher R. L. (1984) Mineralogical studies of the residues of mantle melting: abyssal and alpine-type peridotites. In *Kimberlites II: The Mantle and Crust Relationships* (ed. J. Kornprobst), pp. 295-308. Elsevier.

Dick H. J. B., Fisher R. L., and Bryan W. B. (1984) Mineralogical variability of the uppermost mantle along mid-ocean ridges. *Earth Planet. Sci. Lett.* **69**, 88-106.

Eggins S. M., Woodhead J. D., Kinsley L. P. J., Mortimer G. E., Sylvester P., McCulloch M. T., Hergt J. M., and Handler M. R. (1997) A simple method for the precise determination of >40 trace elements in geological samples by ICPMS using enriched isotope internal standardisation. *Chem. Geol.* **134**, 311-326.

Elliott T., Plank T., Zindler A., White W., and Bourdon B. (1997) Element transfer from slab to volcanic front at the Mariana Arc. *J. Geophys. Res.* **102**, 14991-15019.

Ellison A. J. and Hess P. C. (1986) Solution behavior of +4 cations in high silica melts: petrologic and geochemical implications, *Contrib. Mineral. Petrol.* **94**, 343-351.

Forsythe L. M., Nielsen R. L., and Fisk M. R. (1994) High-field-strength element partitioning between pyroxene and basaltic to dacitic magmas. *Chem. Geol.* **117**, 107-125.

Fujinawa A. and Green T. H. (1997) Partitioning behavior of Hf and Zr between amphibole, clinopyroxene, garnet and silicate melts at high pressure. *Eur. J. Mineral.* **9**, 379-391.

Gaetani G. A. and Grove T. L. (1995) Partitioning of rare earth elements between clinopyroxene and silicate melt; crystal-chemical controls. *Geochim. Cosmochim. Acta* **59**, 1951-1962.

Gallahan W. E. and Nielsen R. L. (1992) The partitioning of Sc, Y, and the rare earth elements between high-Ca pyroxene and natural mafic to intermediate lavas at 1 atmosphere. *Geochim. Cosmochim. Acta* **56**, 2387-2404.

Green T. H. (1981) Experimental evidence for the role of accessory phases in magma genesis. *J. Volcan. Geotherm. Res.* **10**, 405-422.

Green T. H., Sie S. H., Ryan C. G., and Cousens D. R. (1989) Proton microprobe determined partitioning of Nb, Ta, Zr, Sr and Y between garnet, clinopyroxene and basaltic magma at high pressure and temperature. *Chem. Geol.* **74**, 201-216.

Gurenko A. A. and Chaussidon M. (1995) Enriched and depleted primitive melts included in olivine from Icelandic tholeiites: Origin by continuous melting of a single mantle column. *Geochim. Cosmochim. Acta* **59**, 2905-2917.

Hart S. R. and Brooks C. (1974) Clinopyroxene-matrix partitioning of K, Rb, Cs, Sr, and Ba. *Geochim. Cosmochim. Acta* **38**, 1799-1806.

Hart S. R. and Dunn T. (1993) Experimental cpx/melt partitioning of 24 trace elements. *Contrib. Mineral. Petrol.* **113**, 1-8.

Hauri E., Wagner T. P., and Grove T. L. (1994) Experimental and natural partitioning of Th, U, Pb and other trace elements between garnet, clinopyroxene and basaltic melts. *Chem. Geol.* **117**, 149-166.

Hirschman M. M. and Stolper E. M. (1996) A possible role for garnet pyroxenite in the origin of the "garnet signature" in MORB. *Contrib. Mineral. Petrol.* **124**, 185-208.

Hoernle K., Lundstrom C., and Gill J. ^{238}U-^{230}Th-^{226}Ra and ^{235}U-^{231}Pa disequilibria in Canary and Madeira Island volcanic rocks: melting processes beneath intra-plate volcanoes, manuscript in preparation.

Johnson K. T. M. and Kinzler R. J. (1989) Partitioning of REE, Ti, Zr, Hf, and Nb between clinopyroxene and basaltic liquid: an ion microprobe study, *Eos Trans. Amer. Geophys. Union* **70**, 1388.

Johnson K. T. M., Dick H. J. B., and Shimizu N. (1990) Melting in the oceanic upper mantle: an ion microprobe study of diopsides in abyssal peridotites. *J. Geophys. Res.* **95**, 2661-2678.

Kelemen P. B., Kinzler R. J., Johnson K. T. M., and Irving A. J. (1990) High field strength element depletions in arc basalts due to magma-mantle interaction. *Nature* **345**, 521-524.

LaTourette T. Z. and Burnett D. S. (1992) Experimental determination of U and Th partitioning between clinopyroxene and natural and synthetic basaltic liquid *Earth Planet. Sci. Lett.* **110**, 227-244.

LaTourette T., Hervig R. L., and Holloway J. R. (1995) Trace element partitioning between amphibole, phlogopite and basanite melt. *Earth Planet. Sci. Lett.* **135**, 13-30.

Lundstrom C. C., Shaw H. F., Ryerson F. J., Phinney D., Gill J., and Williams Q. (1994) Compositional controls on the partitioning of U, Th, Ba, Pb, Sr and Zr between clinopyroxene and haplobasaltic melts; implications for uranium series disequilibria in basalts. *Earth Planet. Sci. Lett.* **128**, 407-423.

McCallum I. S. and Charette M. P. (1978) Zr and Nb partition coefficients: implications for the genesis of mare basalts, KREEP, and sea floor basalts. *Geochim. Cosmochim. Acta* **42**, 859-869.

McKay G., Wagstaff J., and Yang S.-R. (1986) Clinopyroxene REE distribution coefficients for Shergottites: The REE content of the Shergotty melt. *Geochim. Cosmochim. Acta* **50**, 927-937.

Michael P. J. and Bonatti E. M. (1985) Peridotite composition from the North Atlantic; regional and tectonic variations and implications for partial melting. *Earth Planet. Sci. Lett.* **73**, 91-104.

Mysen B. O., Virgo D., and Seifert F. A. (1985) Relationships between properties and structure of aluminosilicate melts. *Amer. Mineral.* **70**, 88-105.

Niu Y. and Batiza R. (1997) Trace element evidence from seamounts for recycled oceanic crust in the Eastern Pacific mantle. *Earth Planet. Sci. Lett.* **148**, 471-483.

Niu Y. and Hekinian R. (1997a) Spreading rate dependence of the extent of mantle melting beneath ocean ridges. *Nature* **385**, 326-329.

Niu Y. and Hekinian R. (1997b) Basaltic liquids and harzburgitic residues in the Garrett Transform: a case study at fast spreading ridges. *Earth Planet. Sci. Lett.* **146**, 243-258.

Onuma N., Higuchi H., Wakita H., and Nagasawa H. (1968) Trace element partitioning between two pyroxenes and the host lava. *Earth Planet. Sci. Lett.* **5**, 47-51.

Plank T. and White W. M. (1995) Nb and Ta in arc and mid-ocean ridge basalts. *Eos Trans. Amer. Geophys. Union* **76**, F655.

Ray G. L., Shimizu N., and Hart S. R. (1983) An ion microprobe study of the partitioning of trace elements between clinopyroxene and liquid in the system diopside-albite-anorthite. *Geochim. Cosmochim. Acta* **47**, 2131-2140.

Ryerson F. J. and Hess P. C. (1978) Implications of liquid-liquid distribution coefficients to mineral-liquid partitioning. *Geochim. Cosmochim. Acta* **42**, 921-932.

Salters V. J. M. and Shimizu N. (1988) World-wide occurrence of HFSE-depleted mantle. *Geochim. Cosmochim. Acta* **52**, 2177-2182.

Saunders A. D., Tarney J., and Weaver S. D. (1980) Transverse geochemical variation across the Antarctic Peninsula: implications for the genesis of calc-alkaline magmas. *Earth Planet. Sci. Lett.* **46**, 344-360.

Shannon R. D. (1976) Revised effective ionic radii and systematic studies of interatomic distances in halides and chalcogenides. *Acta. Crystallogr.* **A32**, 751-767.

Shimizu N. (1974) An experimental study of the partitioning of K, Rb, Cs, Sr, and Ba between clinopyroxene and liquid at high pressures. *Geochim. Cosmochim. Acta* **38**, 1789-1798.

Skulski T., Minarik W., and Watson E. B. (1994) High pressure experimental trace-element partitioning between clinopyroxene and basaltic melts. *Chem. Geol.* **117**, 127-147.

Smyth J. R. and Bish D. L. (1988) *Crystal Structures and Cation Sites of the Rock-Forming Minerals.* Allen and Unwin.

Sobolov A. V. and Shimizu N. (1993) Ultra-depleted primary melt included in an olivine from the mid-atlantic ridge. *Nature* **363**, 151-154.

Sun S. and McDonough W. F. (1989) Chemical and isotopic systematics of ocean basalts: implications for mantle composition and processes. in *Magmatism in the Ocean Basins* (eds. A.D. Saunders and M.J. Norry), pp 313-345. Blackwell Scientific Publ.

Thirwall M. F., Smith T. E., Graham A. M., Theoforou N., Hollings P., Davidson J. P., and Arculus R. J. (1994) High field strength element anomalies in arc lavas: source or process? *J. Petrol.* **35**, 819-838.

Watson E. B. and Ryerson F. J. (1986) Partitioning of zirconium between clinopyroxene and magmatic liquids of intermediate composition. *Geochim. Cosmochim. Acta* **50**, 2523-2526.

Watson E. B., Othman D. B., Luck J., and Hofmann A. W. (1987) Partitioning of U, Pb, Cs, Yb, Hf, Re, and Os between chromian diopsidic pyroxene and haplobasaltic liquid. *Chem. Geol.* **62**, 191-208.

Weaver B. L. (1991) The origin of ocean island basalt endmember compositions: trace element and isotopic constraints. *Earth Planet. Sci. Lett.* **104**, 381-397.

Wood B. J. and Blundy J. D. (1997) A predictive model for rare earth element partitioning between clinopyroxene and anhydrous silicate melt. *Contrib. Mineral. Petrol.* **129**, 166-181.

Woodhead J., Eggins S., and Gamble J. (1993) High field strength and transition element systematics in island arc and back-arc basin basalts: evidence for multi-phase melt extraction and a depleted mantle wedge. *Earth Planet. Sci. Lett.* **114**, 491-504.

Table 1 Major element compositions of clinopyroxenes and glasses.

	~Di_{65}-An_{35}				~Di_{55}-Ab_{45}			
	starting composition	cpx	glass	F*	starting composition	cpx	glass	F*
n	3	10	8		3	10	10	
SiO_2	49.0	51.6 ±0.4	49.5 ±0.3	-0.23	60.1	55.2 ±0.3	61.3 ±0.5	0.20
TiO_2	1.02	0.40 ±0.03	1.03 ±0.03	0.02	0.97	0.22 ±0.02	1.05 ±0.04	0.10
Al_2O_3	14.4	4.8 ±0.3	14.7 ±0.2	0.03	9.2	0.75 ±0.04	9.6 ±0.1	0.05
Cr_2O_3	0.18	2.1 ±0.2	0.15 ±0.04	0.02	0.2	1.6 ±0.3	0.07 ±0.03	0.06
CaO	23.1	24.5 ±0.2	23.1 ±0.2	0.03	13.2	23.2 ±0.3	12.5 ±0.2	0.06
MgO	10.4	16.4 ±0.2	10.1 ±0.1	0.04	9.0	18.2 ±0.2	8.5 ±0.2	0.06
Na_2O	0.1	0.0 ±0.0	0.05 ±0.02	0.00	5.5	0.54 ±0.09	5.64 ±0.07	0.03
total	98.2	99.8	98.6		98.1	99.8	99.0	
			NBO/T#=	0.93			NBO/T=	0.71

Calculated cation distributions on a 6 oxygen basis:

	T site:		M1:				M2:		
	Si^{+4}	Al^{+3}	Al^{+3}	Cr^{+3}	Ti^{+4}	Mg^{+2}	Ca^{+2}	Mg^{+2}	Na^{+1}
DiAn	1.870	0.130	0.073	0.061	0.011	0.855	0.954	0.032	0.000
DiAb	1.989	0.011	0.021	0.045	0.006	0.928	0.896	0.049	0.041

*F is % crystallization by mass balance #Mysen et al. [1985]

Table 2 Glass trace element contents, partition coefficients and partition coefficient ratio of experiments

	Di_{65}-An_{35}		Di_{55}-Ab_{45}		
	glass (ppm)	$^{cpx/l}D$ (error)	glass (ppm)	$^{cpx/l}D$ (error)	$^{cpx/l}D_{Di\text{-}An}/^{cpx/l}D_{Di\text{-}Ab}$
Na		0.16 (2)		0.10 (2)	1.63
Al		0.32 (2)		0.078 (4)	4.10
Ca		1.06 (1)		1.85 (3)	0.57
Ti		0.39 (3)		0.21 (2)	1.86
Cr		14 (4)		20 (10)	0.70
Rb	210	0.00024 (7)	310	0.00021 (9)	1.17
Sr	103	0.102 (7)	65	0.146 (5)	0.70
Zr	106	0.20 (3)	77	0.045 (5)	4.57
Nb	652	0.006 (1)	662	0.0028 (3)	2.10
Ba	390	0.00024 (5)	422	0.00024 (4)	1.00
La	277	0.063 (5)	352	0.056 (9)	1.11
Nd	316	0.18 (2)	290	0.16 (2)	1.15
Sm	368	0.27 (2)	370	0.22 (3)	1.22
Gd	361	0.28 (3)	360	0.25 (3)	1.14
Yb	358	0.23 (3)	361	0.22 (4)	1.01
Hf	87	0.43 (4)	78	0.09 (2)	5.04
Ta	425	0.019 (5)	373	0.0024 (5)	8.11
Pb	103	0.020 (4)	187	0.017 (2)	1.14
Th	402	0.008 (2)	367	0.0013 (2)	6.33

Numbers in parentheses are 1σ in terms of least units cited and are based on sample standard deviation of 3 to 4 clinopyroxene analyses and 3 to 4 glass analyses. Estimated uncertainty on concentrations is ±20%

Table 3 Comparison of recent high field strength element $^{cpx/l}D$

	Composition	T°C	D_{Zr}	D_{Hf}	D_{Nb}	D_{Ta}	D_{Ti}	D_{Hf}/D_{Zr}	D_{Ta}/D_{Nb}
This study-	$Di_{65}An_{35}$	1275	0.204	0.431	0.0058	0.019	0.388	2.11	3.28
This study-	$Di_{55}Ab_{45}$	1275	0.045	0.086	0.0028	0.0024	0.209	1.91	0.86
McCallum and Charette 1978	basaltic	1105-1128	0.05-0.22		0.01-0.03				
Watson and Ryerson, 1986	intermediate	950-1000	0.27						
Dunn, 1987	basaltic	1250-1290		0.26-0.35			0.35-0.43		
Johnson et al., 1989	basaltic	1240-1355	0.12-0.27	0.24-0.44	0.06		0.41-0.56	~2	
Skulski et al, 1994	alk. basalt	1235-1300	0.089	0.179	0.003	0.01	0.273	2.01	3.33
Forsythe et al., 1994	mafic to intermediate	1170-1270	0.022-1.059		0.004-0.039	0.029-0.164	0.32-1.08		~2-8
Green et al., 1989	basaltic	1100	0.1		0.005	0.013			2.60
Hart and Dunn, 1993	alk. basalt	1380	0.123	0.256	0.077		0.38-0.55	2.08	
Hauri et al., 1994	basaltic	1405-1430	0.195	0.223	0.0081		0.451	1.14	
Watson et al., 1986	haplobasalt	1275		0.36					
Fujinawa and Green, 1997	intermediate and basanitic	900-1050	0.04	0.07-0.39			0.26-0.9	2.2	

Table 4 Calculated Young's Modulii and optimum D using the methods of Blundy and Wood, 1994

	Cation Charge	n[#]	R^2	site[*]	E (kbar)	D_o
This study, DiAn	1+	2		M2	496	0.23
This study, DiAb	1+	2		M2	469	0.14
Blundy and Wood	1+			M2	504	
This study, DiAn	2+	3	1.000	M2	1551	1.56
This study, DiAb	2+	3	1.000	M2	1645	2.77
Blundy and Wood	2+			M2	1465	
This study, DiAn	3+	4	0.992	M2	2979	0.30
This study, DiAb	3+	4	0.999	M2	2924	0.27
Blundy and Wood	3+			M2	3956	
This study, DiAn	4+	3	0.997	M1[&]	34,015	2.50
This study, DiAb	4+	3	0.998	M1[&]	28,494	0.65

[#] number of points used in regression

[*] r_o for M2 site based on eqn. 15 of Wood and Blundy, 1997

[&] r_o=0.66 for Di-An and 0.652 for Di-Ab by best fit

Figure 1(a). A representative photomicrograph of a clinopyroxene from the Di_{55}-Ab_{45} experiment showing typical euhedral faces of the clinopyroxenes in the experiments. The line AB denotes the electron microprobe traverse shown in b. The darker area of the picture at lower left is the epoxy mount. (b). Electron microprobe traverse across the clinopyroxene of Fig. 1a showing the relatively small degree of zoning found in these experiments.

Fig. 2. Changes in pyroxene composition within clinopyroxenes of the DiAn experiment as a function of Si cations. Cation proportions based on 6 oxygen basis. Total Al cations change as a function of Si cations but octahedral Al shows no variation implying that changes in Al_2O_3 content of clinopyroxenes solely reflect variations in tetrahedral Al (^{IV}Al) in the DiAn composition. Cr and Ti also negatively correlate with Si indicating a coupling between Cr, ^{IV}Al, and Ti.

Fig. 3. The ratio of a partition coefficient from the Di-An system to one from the Di-Ab system as a function of the field strength of an element. Note the increase in the cpx-melt partitioning of high field strength elements in the DiAn system relative to the DiAb system.

Fig. 4. The partition coefficients of high field strength elements as a function of the Al_2O_3 content of clinopyroxene. Previous results for D_{Th} and D_{Zr} from Lundstrom et al. [1994] plotted as open triangles. Each new data point represents a single ion probe analysis. Al/Si from the ion probe is converted to Al_2O_3 using the calibration curve obtained by the Al/Si observed in the two melt compositions forced to pass through the origin. The strong influence of aluminum on the partitioning of these elements is observed over both the range of compositions within all experiments and within the individual spots of one experiment. The inset shows a blow up of the changes in D_{Zr} with changing Al_2O_3 in the DiAn experiment. Because Fig. 2 clearly demonstrates that changes in Al_2O_3 solely reflect variation in ^{IV}Al, the increase in HFSE partitioning reflects variations in ^{IV}Al.

Fig. 5 D_{Nb} as a function of D_{Ta}. Results of ion probe analyses on individual spots. D_{Ta} and D_{Nb} show good correlation as expected but surprisingly do not give a slope of one (line shown), indicating that fractionation of Nb from Ta can occur during clinopyroxene-melt partitioning. The inset shows the results of experimental determinations of D_{Ta}/D_{Nb} as a function of the ^{IV}Al (6 oxygen basis). Only results for non-sector zoned clinopyroxenes from Skulski et al. (1994) used. Results of Forsythe et al. (1994) limited to experiments where the combined relative error (based on reported crystal and melt content errors) does not exceed 70%. Because Nb and Ta require the same charge balancing mechanism, charge balancing cannot be responsible for this relation

implying that discrimination of Nb and Ta in the M1 site (Nb-Ta fractionation) is a function of site size changes related to variations in ^{IV}Al.

Fig. 6 Variation of clinopyroxene-melt partition coefficients as a function of ionic radius for the two compositions. Partition coefficient-ionic radius curves represent the calculated partition coefficients as a function of ionic radius based on site size energetics [Blundy and Wood, 1994] using D_o and E derived from linear regressions (see text). The fits for each curve are excellent (Table 4).

Fig. 7(a) Nb/Ta vs. Nb. Recent high precision ICP-MS data for oceanic basalts (MORB, near ridge seamounts and island arc basalts) show a decrease in Nb/Ta as Nb concentration decreases, most easily explained as melts derived from previously depleted sources [Plank and White, 1995]. The depleted endmember melt can be modeled as the second of two batch melts (12% each) from an originally primitive mantle [Sun and McDonough, 1989] using the partition coefficients determined in the DiAn composition (spinel lherzolite starting and melting modes after Johnson et al., [1990]; mantle cpx mode decreased from 12% to 6% for second melting event with olivine mode correspondingly increased; opx and olivine partition coefficients from Johnson et al. [1990] except D_{Zr} and D_{Ti} which were from Kelemen et al. [1990] and the following estimated values: $^{opx/l}D_{Nb,Ta} = 0.003$, $^{opx/l}D_{Hf} = 0.1$, $^{ol/l}D_{Nb,Ta} = 0.0005$, $^{ol/l}D_{Hf} = 0.01$). The observed range in Nb/Ta is consistent with a mix between a melt from previously depleted mantle and an OIB-like melt (representative of an enriched vein melt) [Sun and McDonough, 1989]. The entire range in these primitive basalts may be explained as a 0-2% pollution of the most depleted melt observed by an OIB-like melt while average NMORB would reflect 5-10% contamination.

(b). Zr/Hf vs. Zr. Near ridge seamount data [Niu and Batiza, 1997] show that Zr has been fractionated from Hf during mantle depletion. Like Nb/Ta, the observed depleted endmember basalt can be modeled as the second of two batch melts (12% each) from an originally primitive mantle [Sun and McDonough, 1989) using the partition coefficients determined in the DiAn composition (and the same model as above). The observed range of Zr/Hf is consistent with a mix between this depleted melt and a small amount of an assumed enriched material (see text).

(c.) Nb/Ta vs. La/Nb. Melting of spinel lherzolite using the DiAn partition coefficients of this study with the same model can account for the depleted basalts of the seamount data of Niu and Batiza [1997] and can produce La/Nb values approaching those observed in the Mariana arc [Elliott et al., 1997]. Although it is often assumed that mantle peridotite producing MORB is distinct from the peridotite source for arcs, upper mantle peridotite beneath ridges and arcs may be quite similar having La/Nb of 4-6. However, normal MORB have lower La/Nb and higher Nb/Ta

due to the input of melts from enriched mafic veins within the MORB source. Arc sources may have had this vein component removed through prior melting in the back arc [Woodhead et al., 1993] such that the HFSE anomaly of the peridotite (high La/Nb) is preserved in arc magmas (although another arc component is also required).

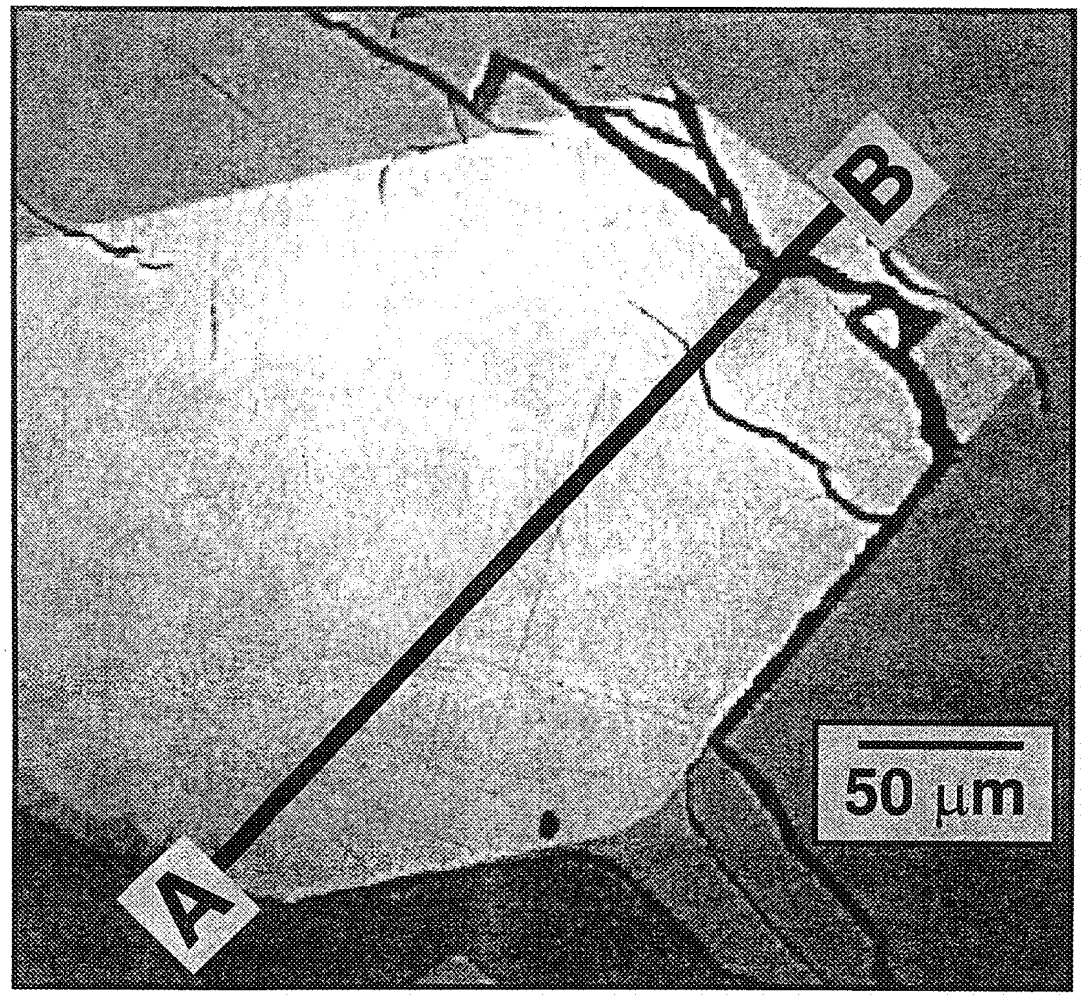

Fig 1a

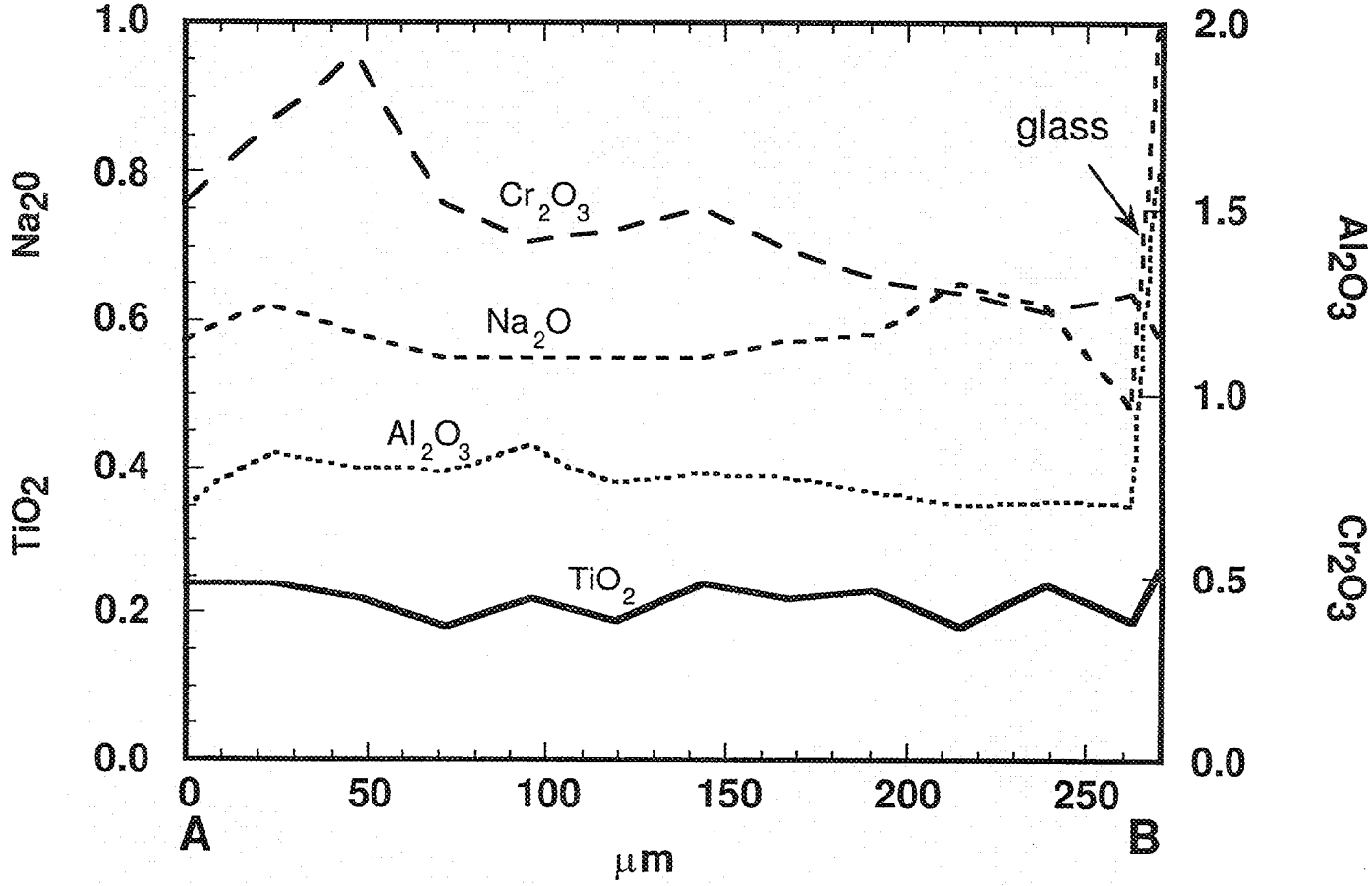
1.0
0.8
0.6
0.4
0.2
0.0
Na2O
TiO2
2.0
1.5
1.0
0.5
0.0
Al2O3
Cr2O3
glass
Cr2O3
Na2O
Al2O3
TiO2
0
50
100
150
200
250
A
B
µm

Fig 1B

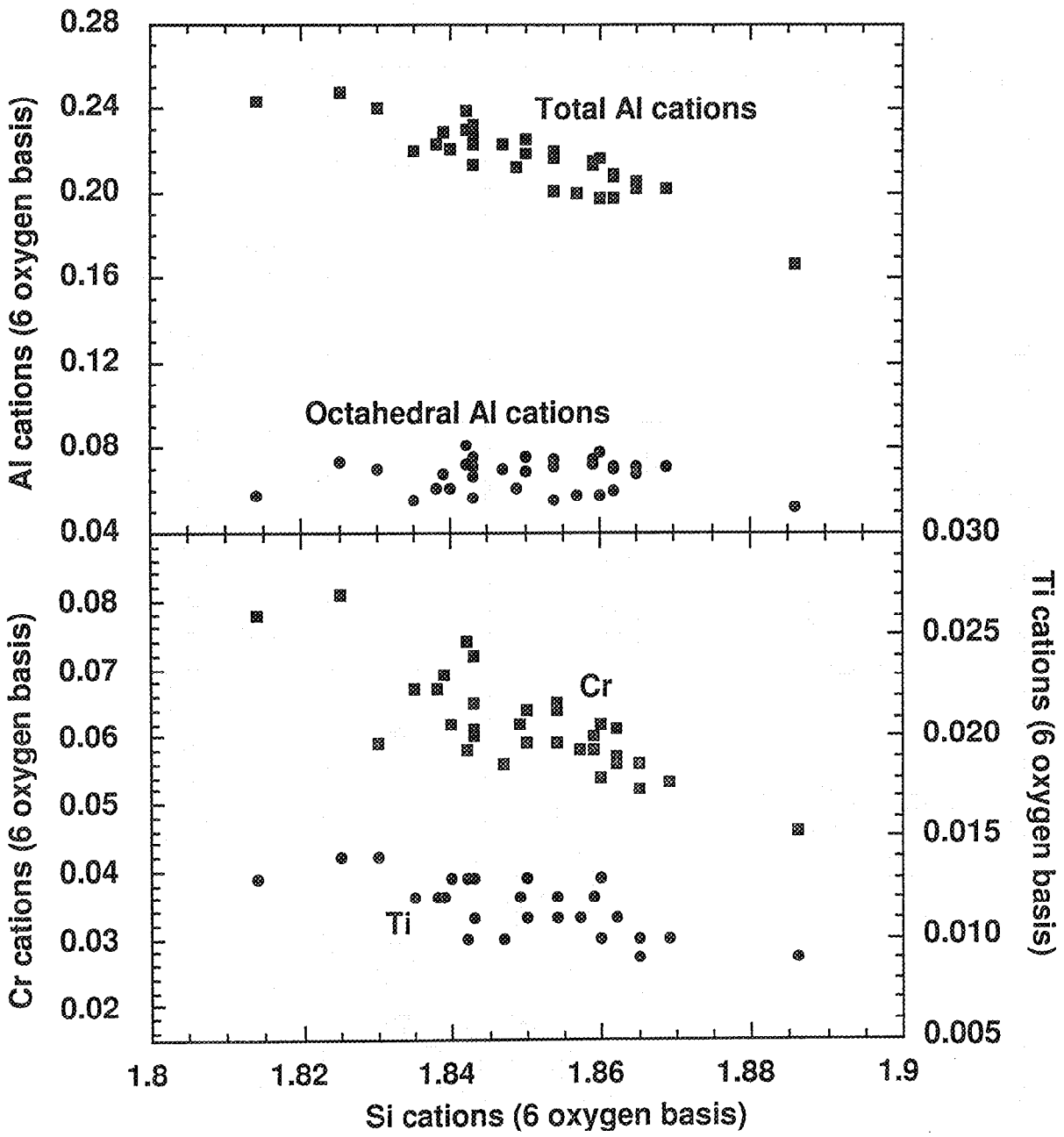
Total Al cations
Octahedral Al cations
Cr
Ti
Al cations (6 oxygen basis)
Cr cations (6 oxygen basis)
Ti cations (6 oxygen basis)
Si cations (6 oxygen basis)
0.28
0.24
0.20
0.16
0.12
0.08
0.04
0.08
0.07
0.06
0.05
0.04
0.03
0.02
0.030
0.025
0.020
0.015
0.010
0.005
1.8
1.82
1.84
1.86
1.88
1.9

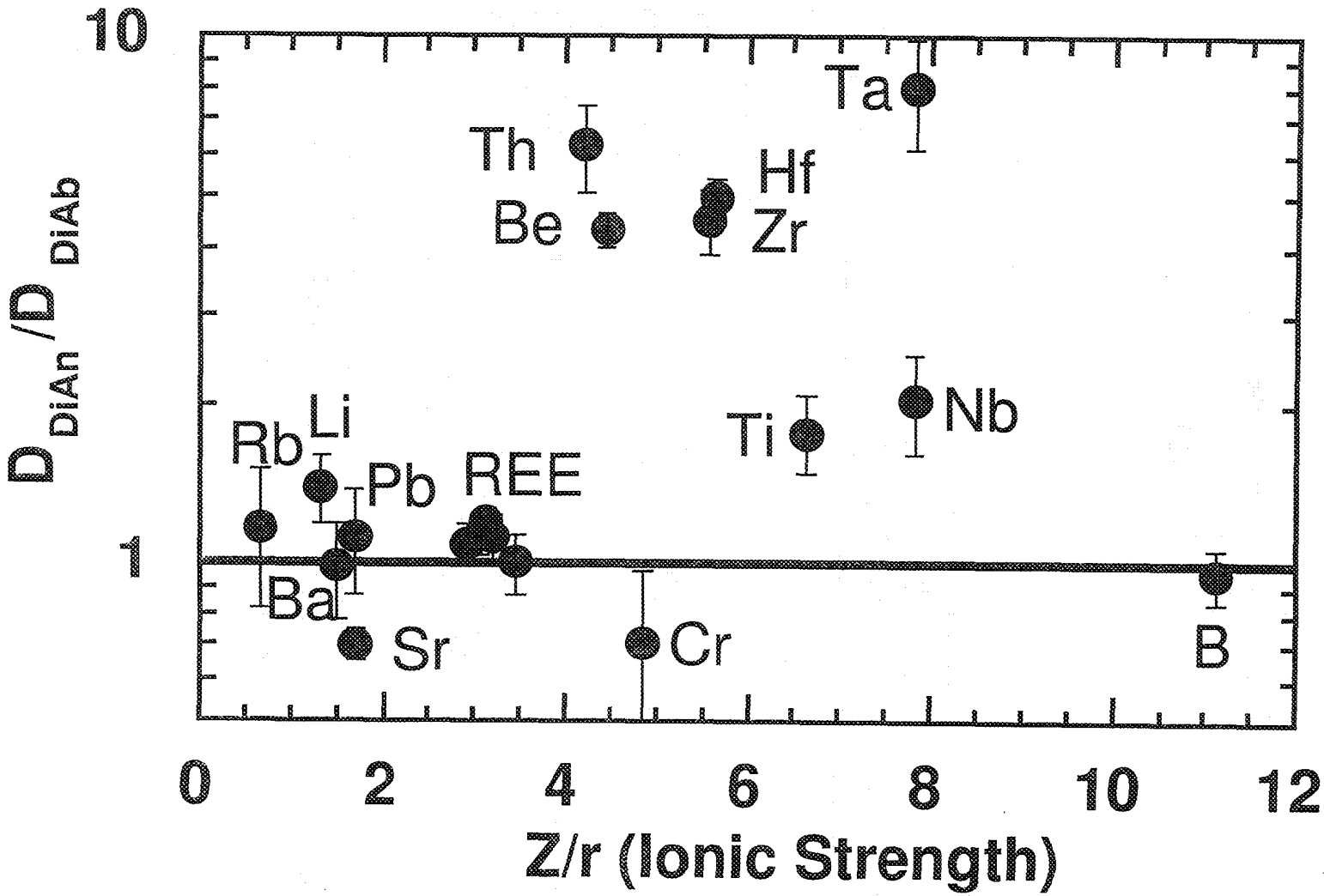
10
1
D_{DiAn}/D_{DiAb}
Th
Be
Hf
Zr
Ta
Ti
Nb
Rb
Li
Pb
REE
Ba
Sr
Cr
B
0
2
4
6
8
10
12
Z/r (Ionic Strength)

Fig 3

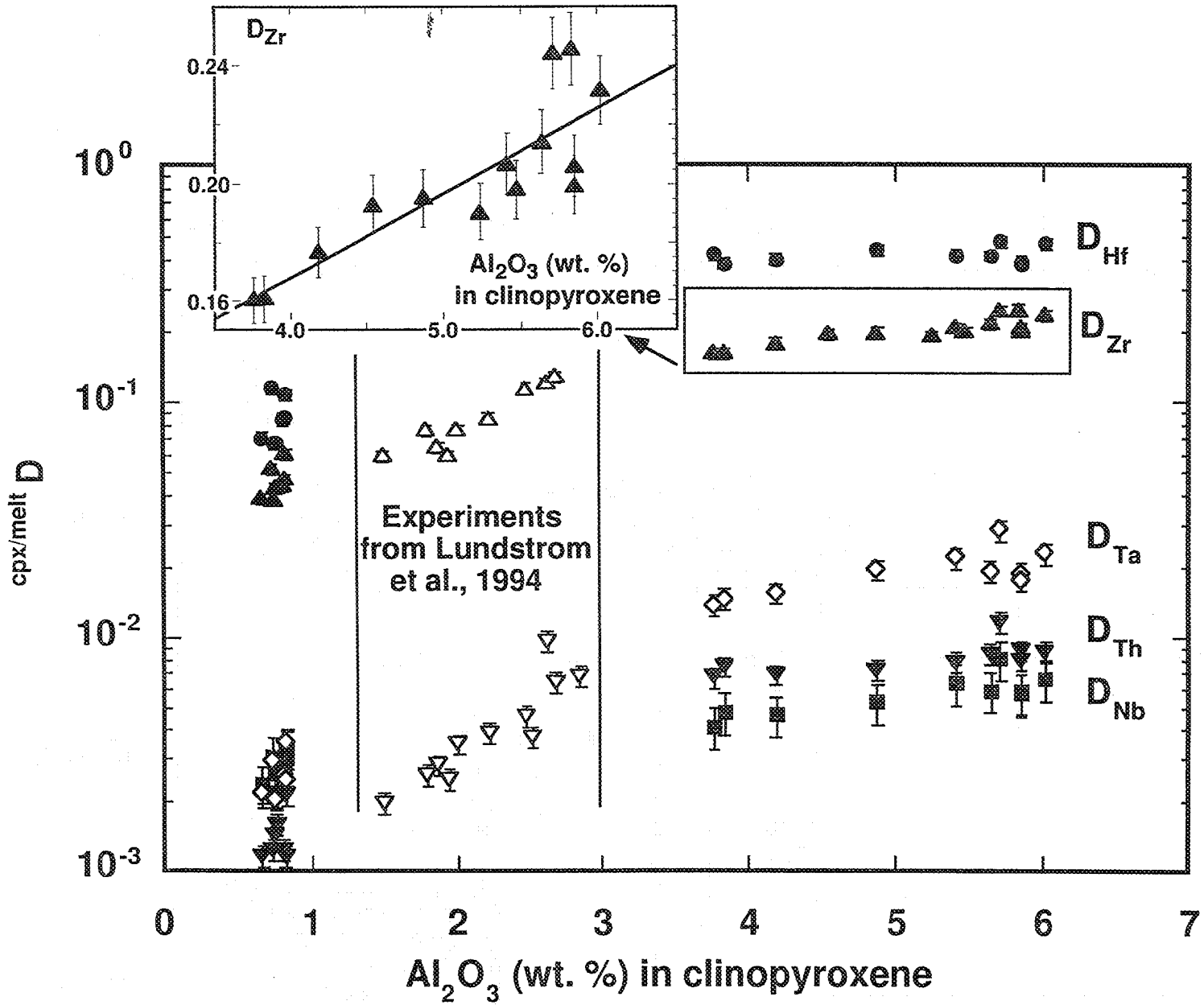
D_Zr
0.24
0.20
0.16
4.0
5.0
6.0
Al2O3 (wt. %)
in clinopyroxene
10^0
10^-1
10^-2
10^-3
cpx/melt D
Experiments
from Lundstrom
et al., 1994
D_Hf
D_Zr
D_Ta
D_Th
D_Nb
0
1
2
3
4
5
6
7
Al2O3 (wt. %) in clinopyroxene

Fig 4

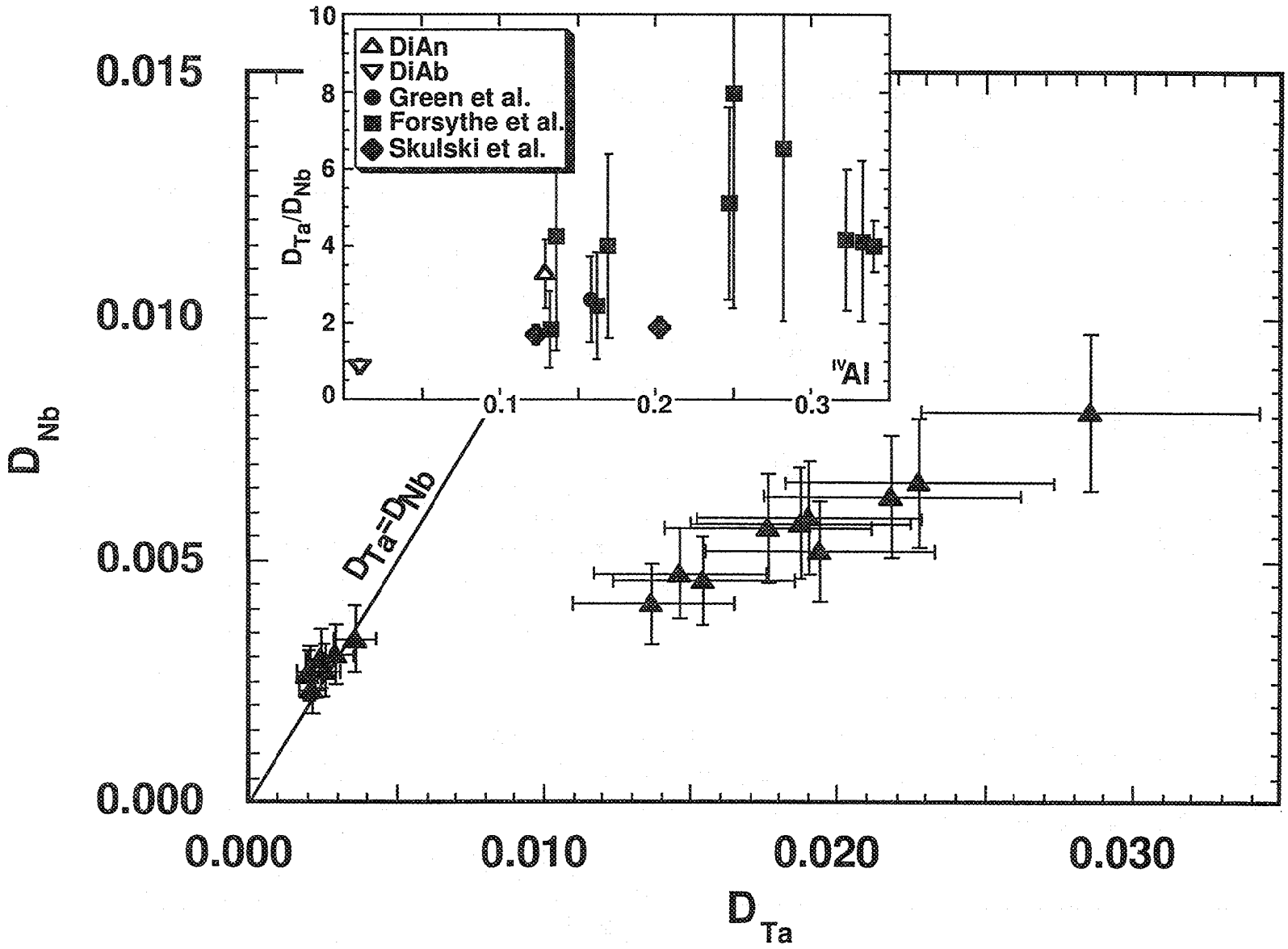
DiAn
DiAb
Green et al.
Forsythe et al.
Skulski et al.
D_{Ta}/D_{Nb}
^{IV}Al
$D_{Ta}=D_{Nb}$
D_{Nb}
D_{Ta}
0.000
0.005
0.010
0.015
0.020
0.030
0
2
4
6
8
10
0.1
0.2
0.3

Fig 5

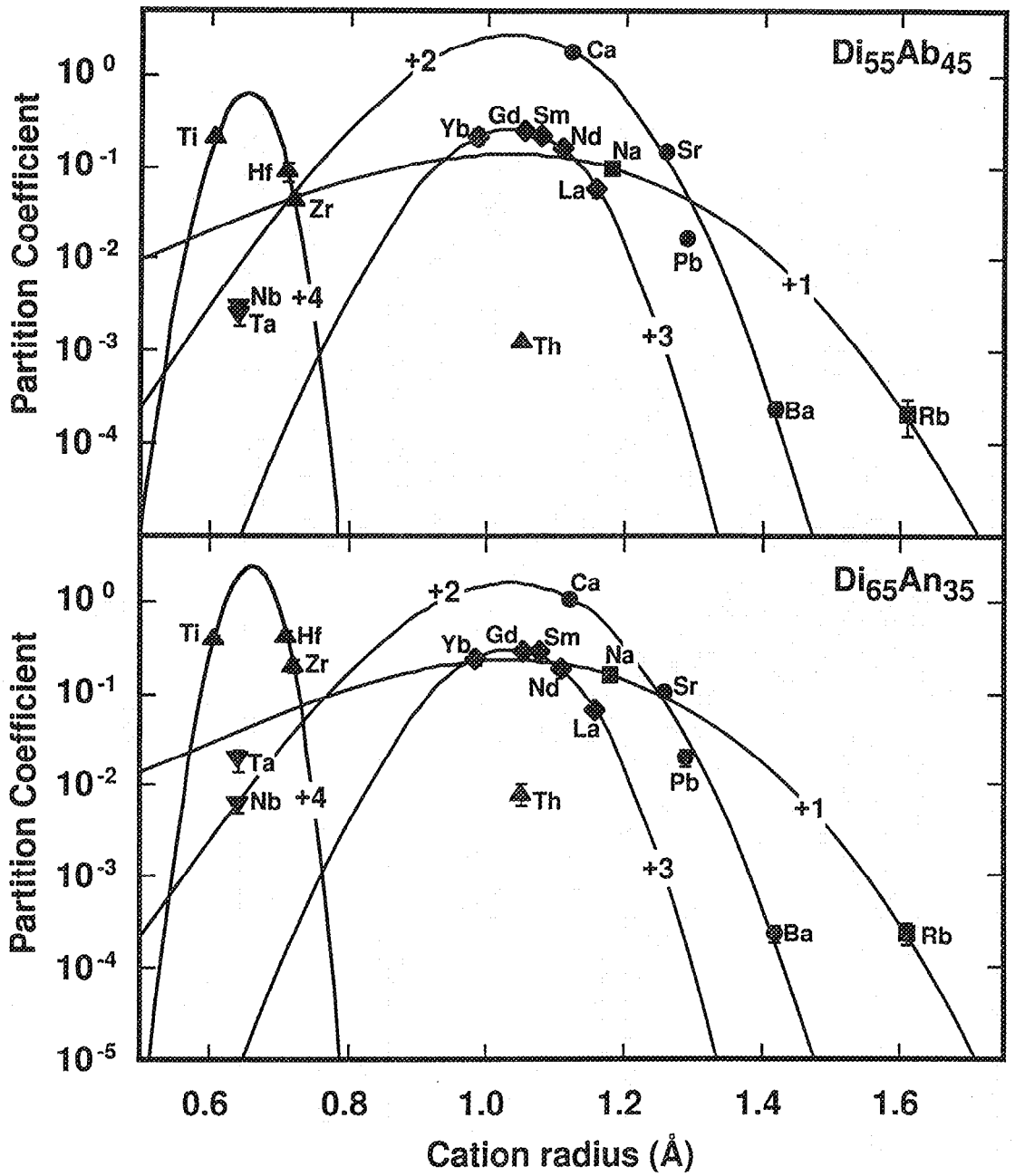
Di55Ab45
Di65An35
Partition Coefficient
Cation radius (Å)
10 0
10 -1
10 -2
10 -3
10 -4
10 -5
0.6
0.8
1.0
1.2
1.4
1.6
+2
+3
+4
+1
Ca
Sr
Na
Ba
Rb
Pb
La
Nd
Sm
Gd
Yb
Th
Ti
Hf
Zr
Nb
Ta

Fig 1

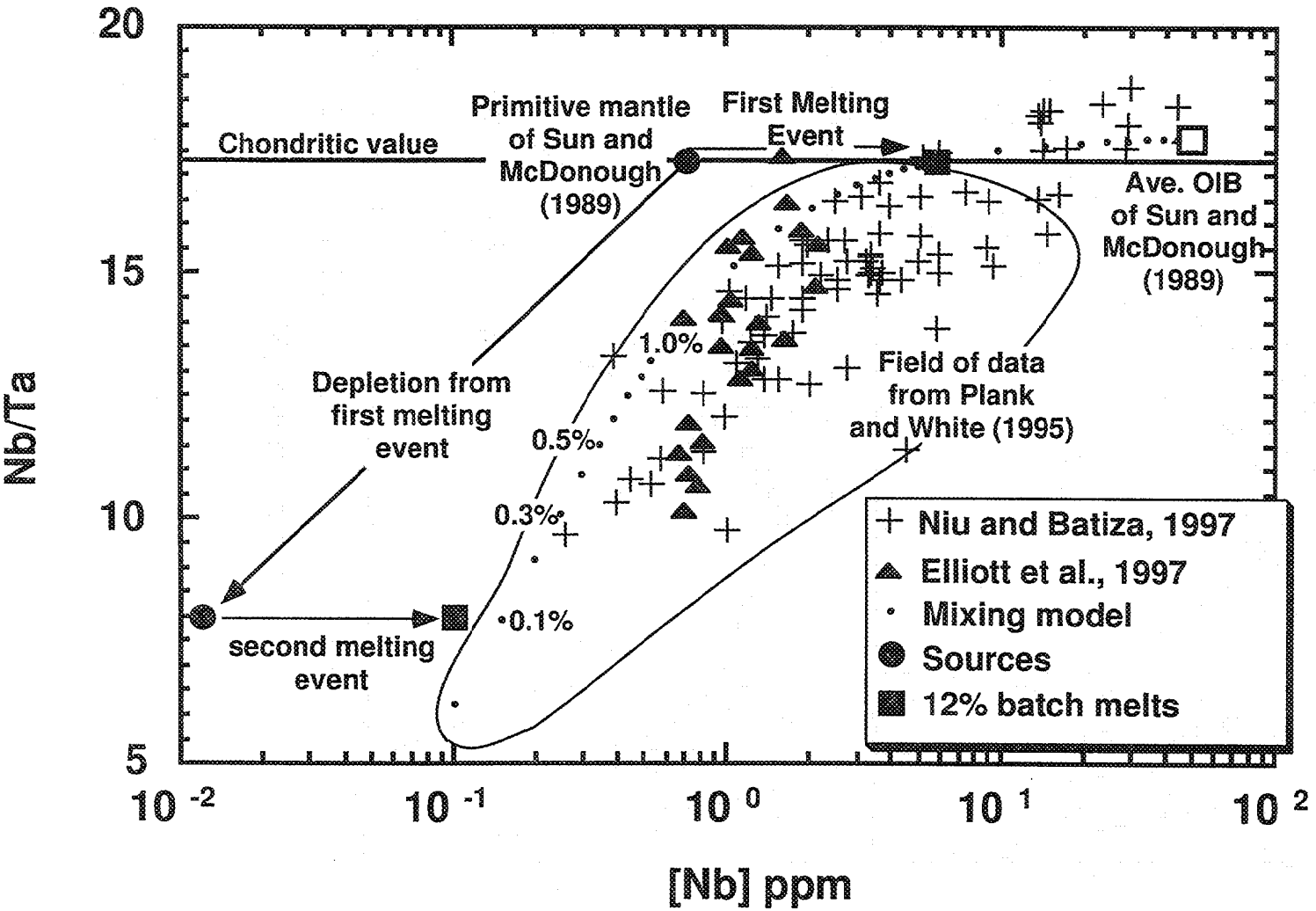
20
15
10
5
Nb/Ta
10 -2
10 -1
10 0
10 1
10 2
[Nb] ppm
Chondritic value
Primitive mantle of Sun and McDonough (1989)
First Melting Event
Ave. OIB of Sun and McDonough (1989)
Depletion from first melting event
1.0%
0.5%
0.3%
0.1%
Field of data from Plank and White (1995)
second melting event
Niu and Batiza, 1997
Elliott et al., 1997
Mixing model
Sources
12% batch melts

Fig. 7a

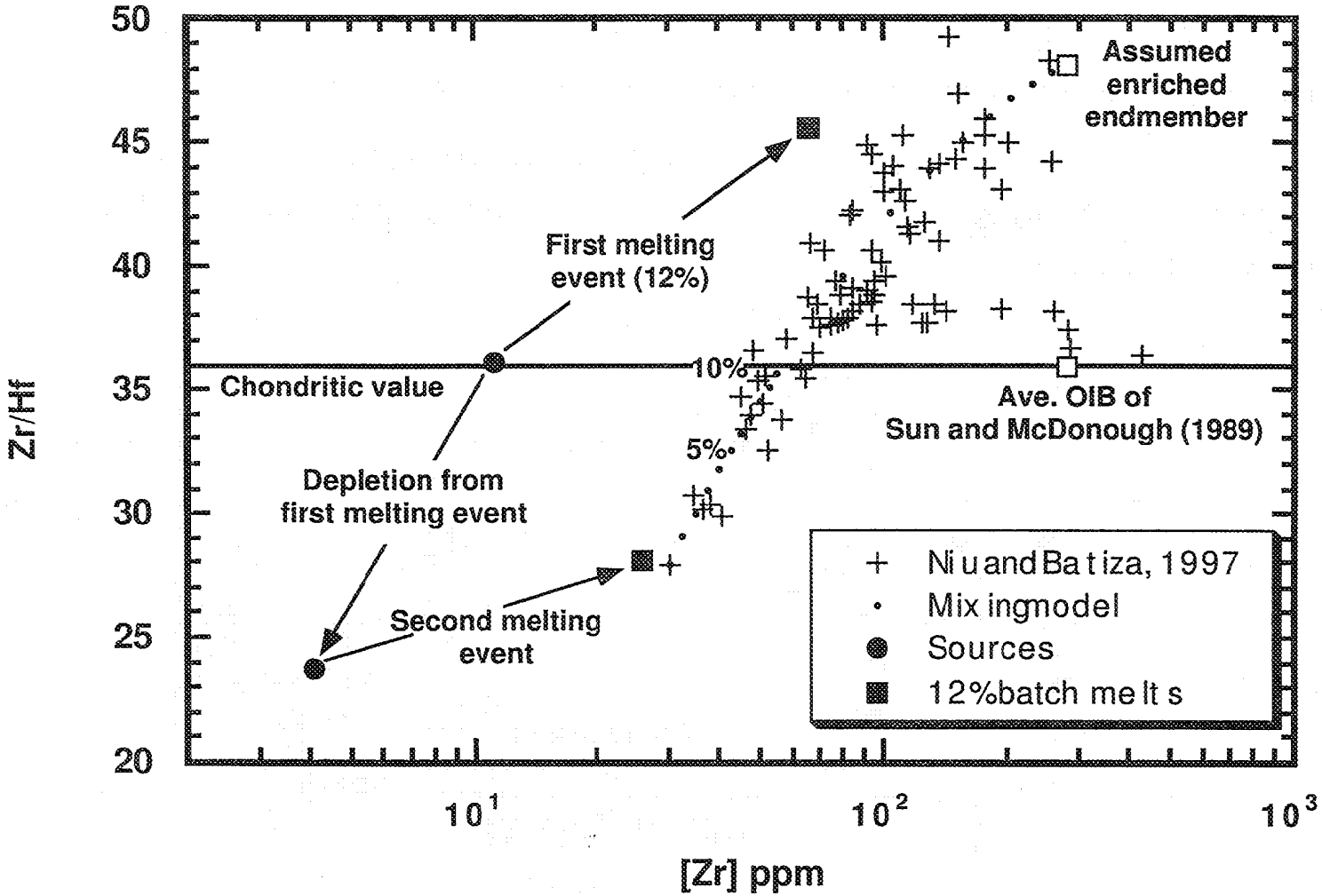
50
45
40
35
30
25
20
Zr/Hf
10^1
10^2
10^3
[Zr] ppm
Assumed enriched endmember
First melting event (12%)
Chondritic value
10%
5%
Ave. OIB of Sun and McDonough (1989)
Depletion from first melting event
Second melting event
Niu and Batiza, 1997
Mixing model
Sources
12% batch melts

Fig. 7b

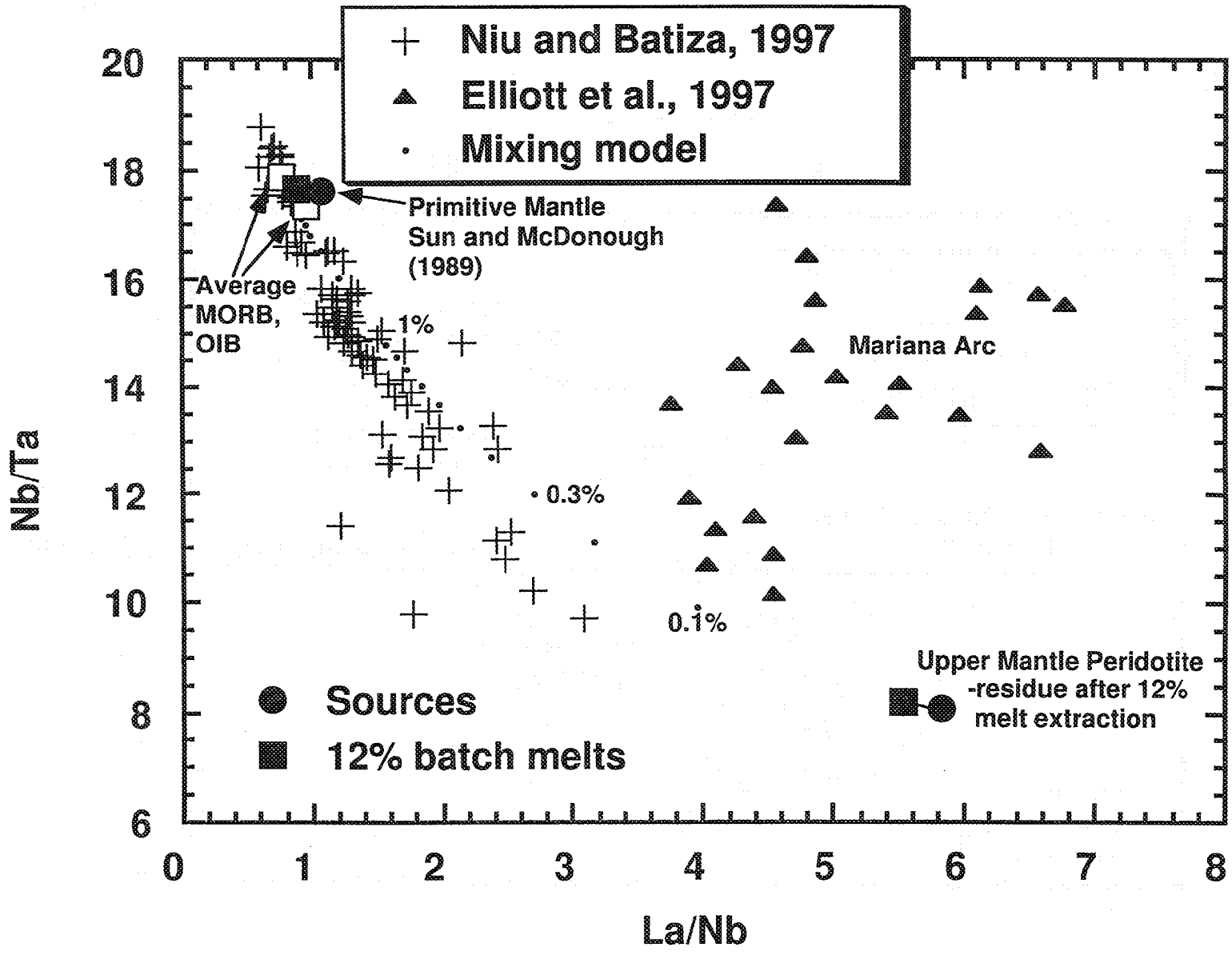
Niu and Batiza, 1997
Elliott et al., 1997
Mixing model
Primitive Mantle
Sun and McDonough
(1989)
Average
MORB,
OIB
1%
0.3%
0.1%
Mariana Arc
Sources
12% batch melts
Upper Mantle Peridotite
-residue after 12%
melt extraction
Nb/Ta
La/Nb
20
18
16
14
12
10
8
6
0
1
2
3
4
5
6
7
8

Fig 7c